

Predicting Microstructure-Creep Resistance Correlation in High Temperature Alloy over Multiple Time Scales

Prof. Vikas Tomar (PI) & Hongsuk Lee & Sudipta Biswas

School of Aeronautics and Astronautics, Purdue University

Prof. Jian Luo (co-PI), Naixie Zhou & Tao Hu (partial supports)

Other UCSD (No-Cost) Contributors: Yuanyao Zhang & Mingde Qin

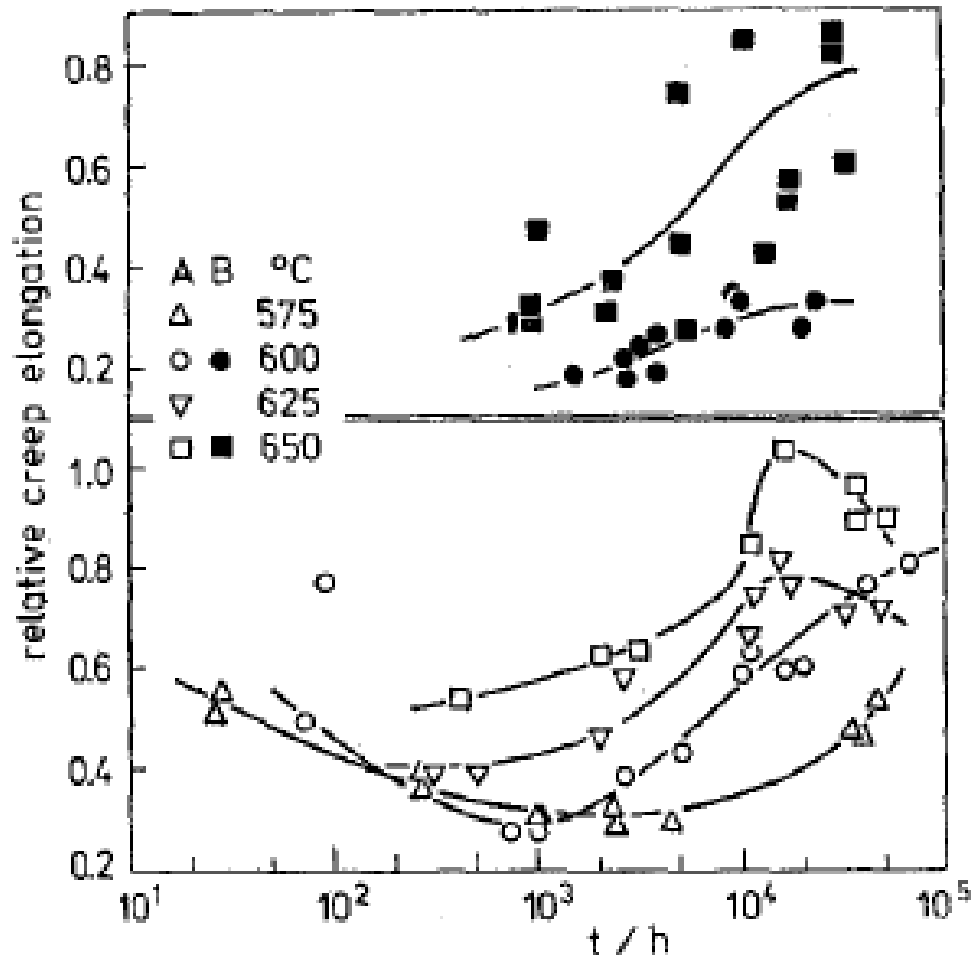
University of California, San Diego & Clemson University

Program Manager: Dr. Jason Hissam

Grant No. : DEFE0011291



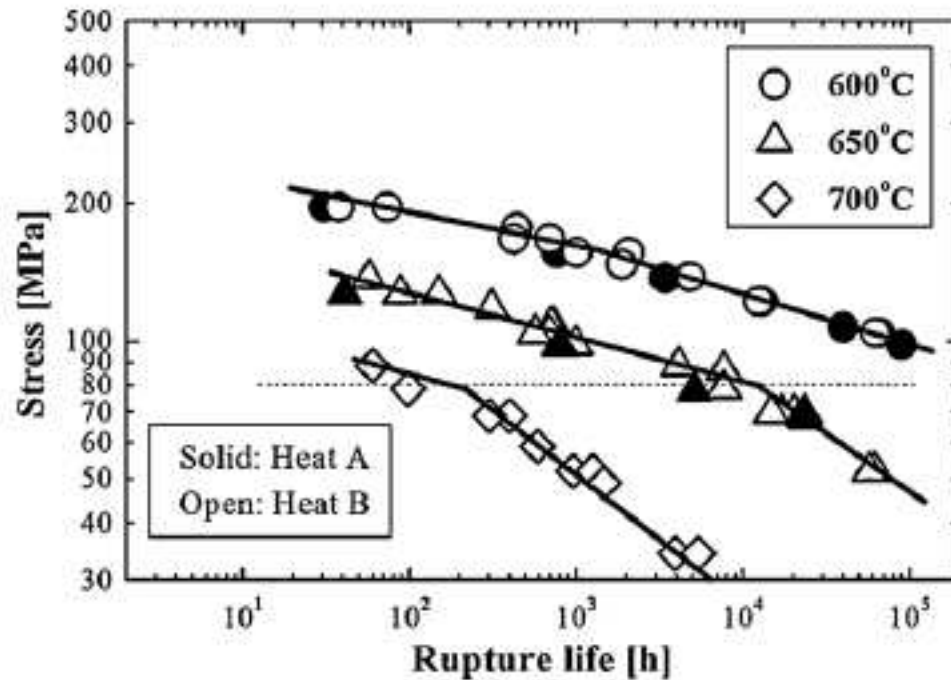
Long Term Creep in Microstructures



Sobotka, 1985, AISI 316 LN Steel

A detailed analysis of microstructure and fractures showed that the developing intergranular precipitation and the following coarsening of grain boundary particles of $M_{23}C_6$, Cr_2N and especially of the sigma phase are responsible for the significant changes of both creep and impact fractures from the point of view of their plasticity.

Long Term Creep in Microstructures

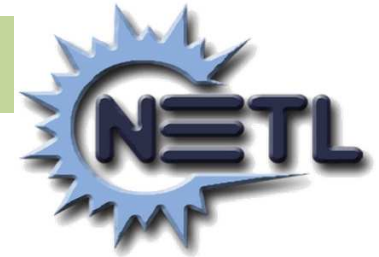


Igarashi, 2011

Fig. 1. Stress and temperature dependence of creep rupture life in Gr.91 steel.

The cause of the breakdown of creep strength has been studied in Gr.91 steel. The results show that the contribution of the static recovery of subgrains to creep deformation causes the breakdown of creep strength. The subgrain boundaries are mainly stabilized by $M_{23}C_6$ and MX precipitates. MX precipitates are thermally stable even in the time range when coarsening of subgrains takes place. Whereas $M_{23}C_6$ precipitates are not thermally stable and the aggregation of $M_{23}C_6$ precipitates takes place in the time range when coarsening of subgrains happens. Therefore, loss of pinning force from $M_{23}C_6$ precipitates is responsible for the static recovery of subgrains. MX has nothing to do with the static recovery. The

Proposal Research Workflow



Task-3

**Theoretical Framework to
Characterize GB Segregation**

Task-1

**Nanocrystalline Ni and Bulk W
Based Alloy Control Sample
Preparation**

Task-4

**Microstructure Level Multiscale
Modeling to Predict Effect of GBs on
Embrittlement, Creep, and rupture**

Task-2

**In-Situ Microstructural Testing of GB
Evolution and Strength**



U.S. DEPARTMENT OF
ENERGY

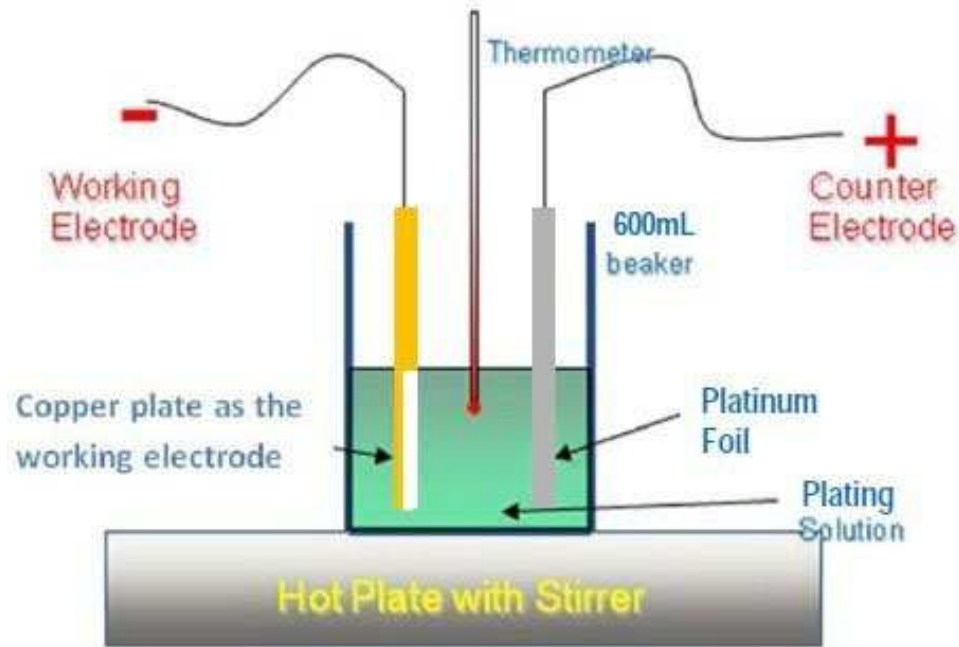
Task 1 (UCSD):
Fabrication and Characterization
of Controlled Specimens

- **Task 1-A: Nanocrystalline Ni-W Binary Alloys (Foil, Synthesized by Electrodeposition)**
- **Task 1-B: Bulk W based Binary Alloy Specimens (Synthesized by High-Energy Ball Milling and Spark Plasma Sintering)**

Task 1-A (UCSD):

Electrodeposited Nanocrystalline Ni-W Specimens

New Ni-W Binary Compositions & Specimens in the Last Year (2015-2016)



Recipe for Preparing Ni-W Binary Nanocrystalline Alloys:

Electrodeposition
Precursor
Solution

$\text{NiSO}_4 \cdot 6\text{H}_2\text{O}$	0.12 mol/L
NaBr	0.3 mol/L
$\text{Na}_3\text{C}_5\text{H}_6\text{O}_7 \cdot 2\text{H}_2\text{O}$	0.6 mol/L
$\text{Na}_2\text{WO}_7 \cdot 2\text{H}_2\text{O}$	0.28 mol/L
NH_4Cl	1 mol/L

Bath Temperature: 75 °C

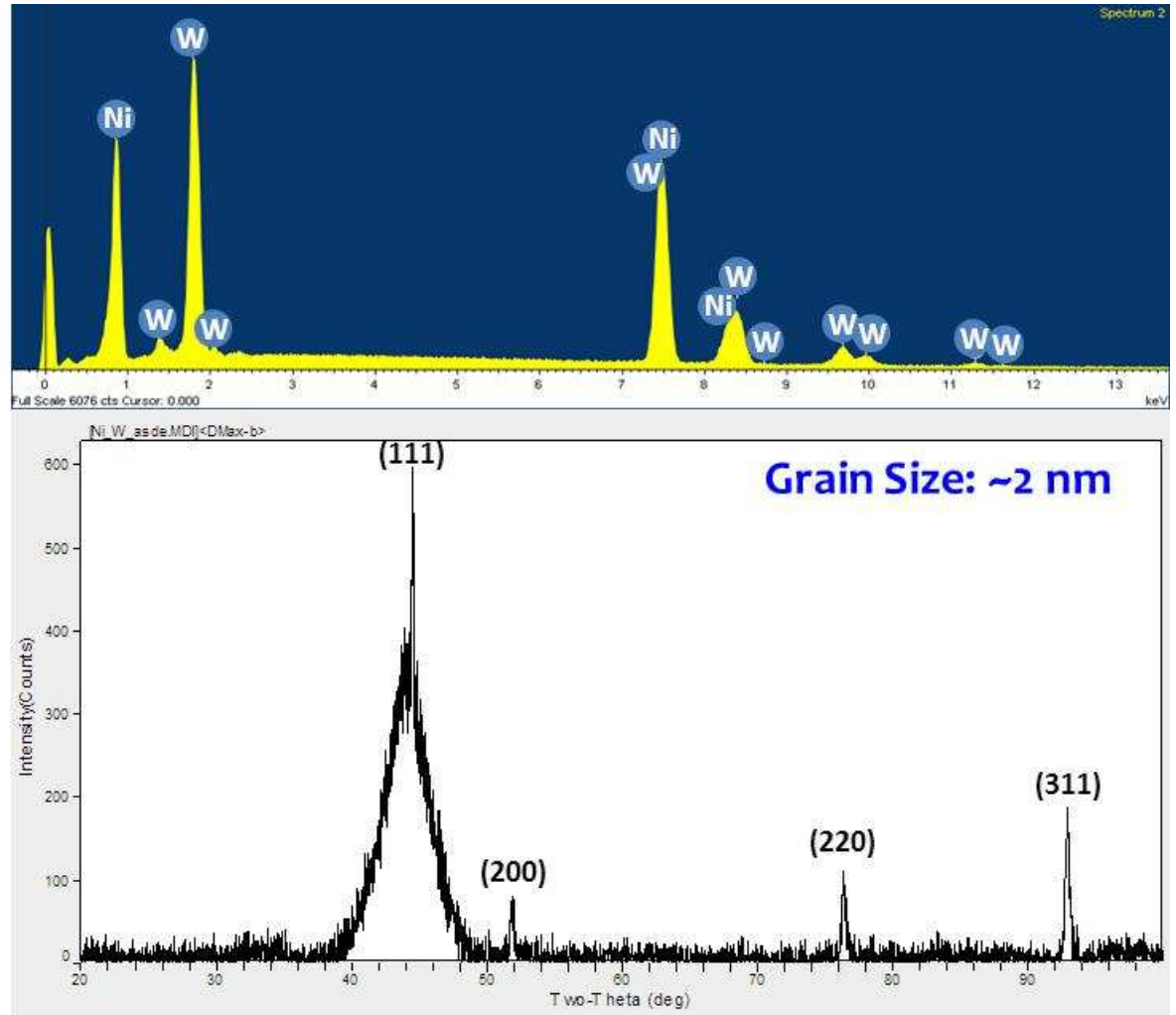
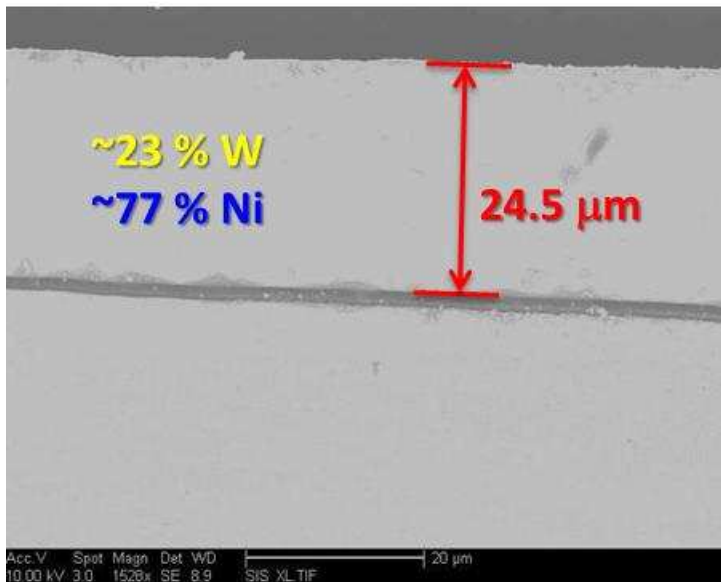
Deposition Time: 30 min

Current	Duration (ms)	Density (A/cm^2)
Forward	20	0.2
Reverse	3	0.1

Task 1-A (UCSD):

Electrodeposited Nanocrystalline Ni-W Specimens

New Ni-W Binary Compositions & Specimens in the Last Year (2015-2016)

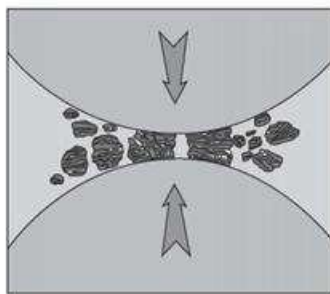


Further Annealing to Adjust Grain Size...

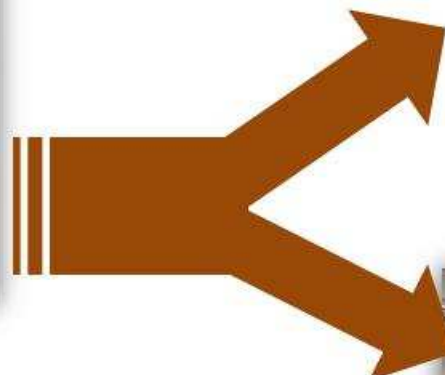
Task 1-B (UCSD):

Bulk W based Binary Alloy Specimens

Synthesized by High-Energy Ball Milling → Pressureless/Spark Plasma Sintering



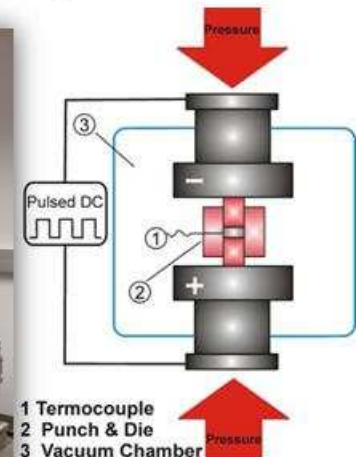
High-Energy Ball Milling



Pressureless Sintering

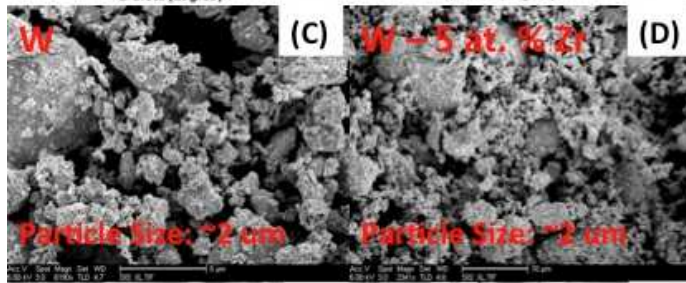
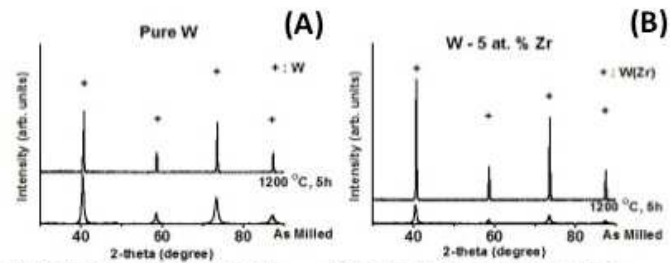


Spark Plasma Sintering

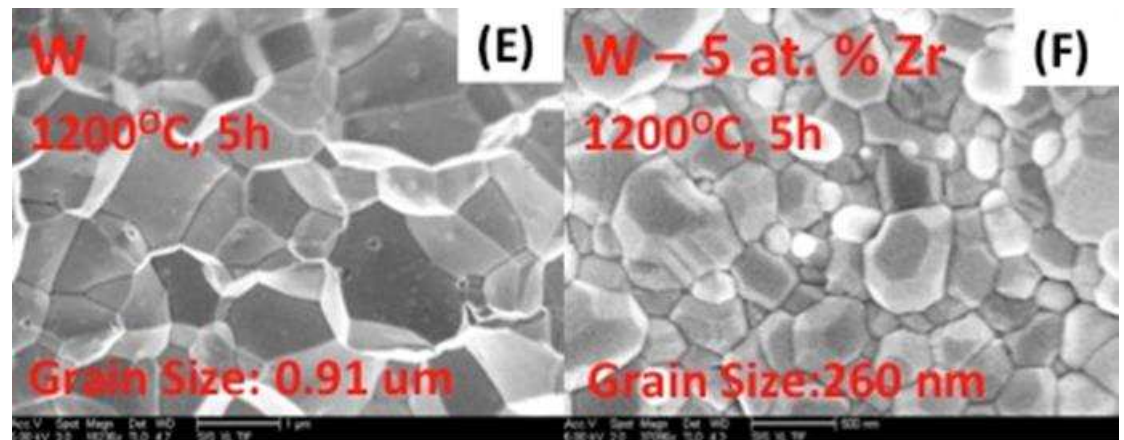


Task 1-B (UCSD):
Pure vs. Zr-doped W:
High-Energy Ball Milling → Pressureless Sintering

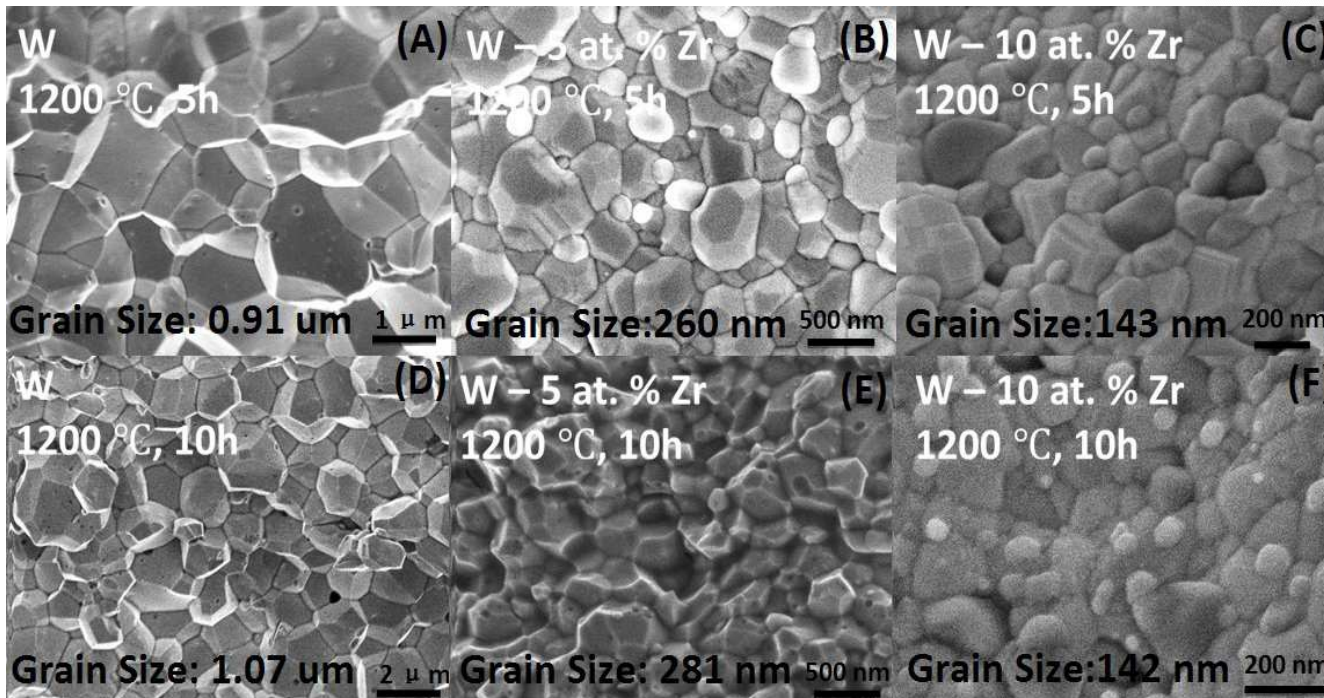
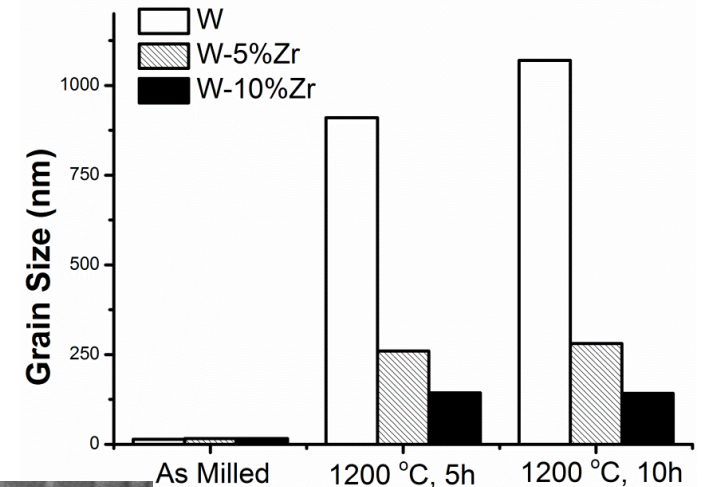
High-Energy Ball Milled Powders



Pressureless Sintered Specimens



Task 1-B (UCSD):
Pure vs. Zr-doped W:
Spark Plasma Sintering (SPS)



Enhanced Thermal Stability of Nanocrystalline W via GB Segregation of Zr!

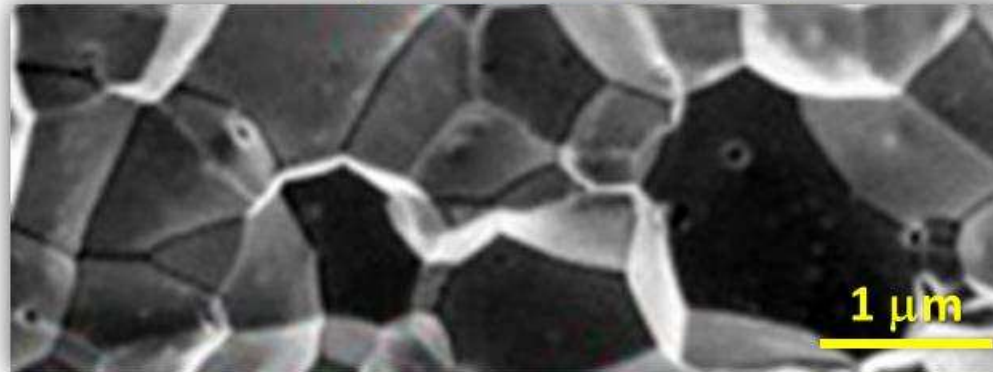
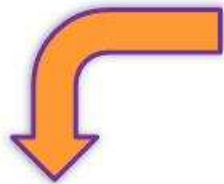
Slower GB kinetics \rightarrow Reduced Coble Creep Rates?

Task 1-B (UCSD):

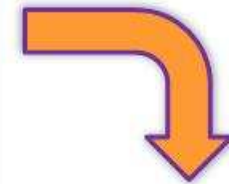
**Pressureless Sintering (1200 °C × 5 hrs):
Pure vs. Re-, Zr-, Co-, Ni-, and Cu-doped W Specimens**

Pure W (Grain Size = ~910 nm)

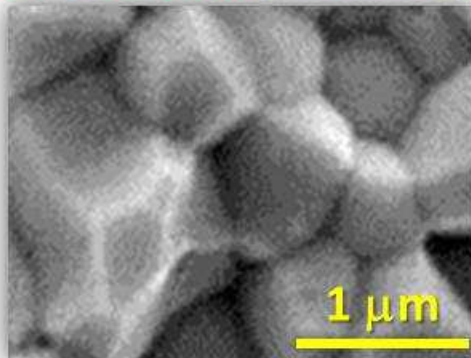
Decreasing
Grain Size



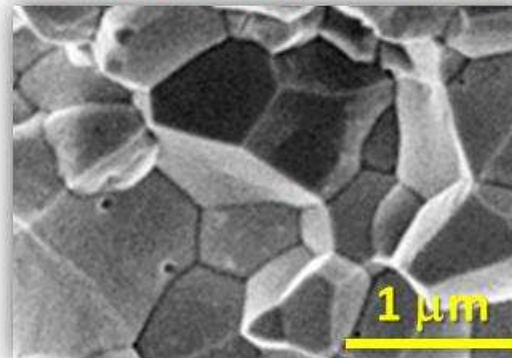
Increasing
Grain Size



W - 5 at. % Ni (~820 nm)



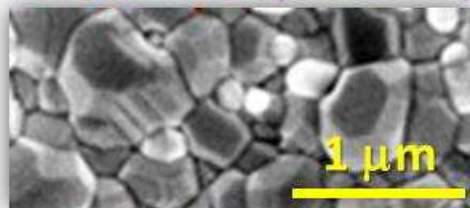
W - 5 at. % Co (~600 nm)



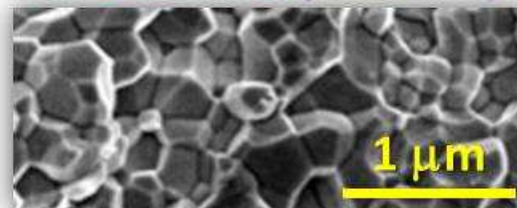
W - 5 at. % Cu (~2200 nm)



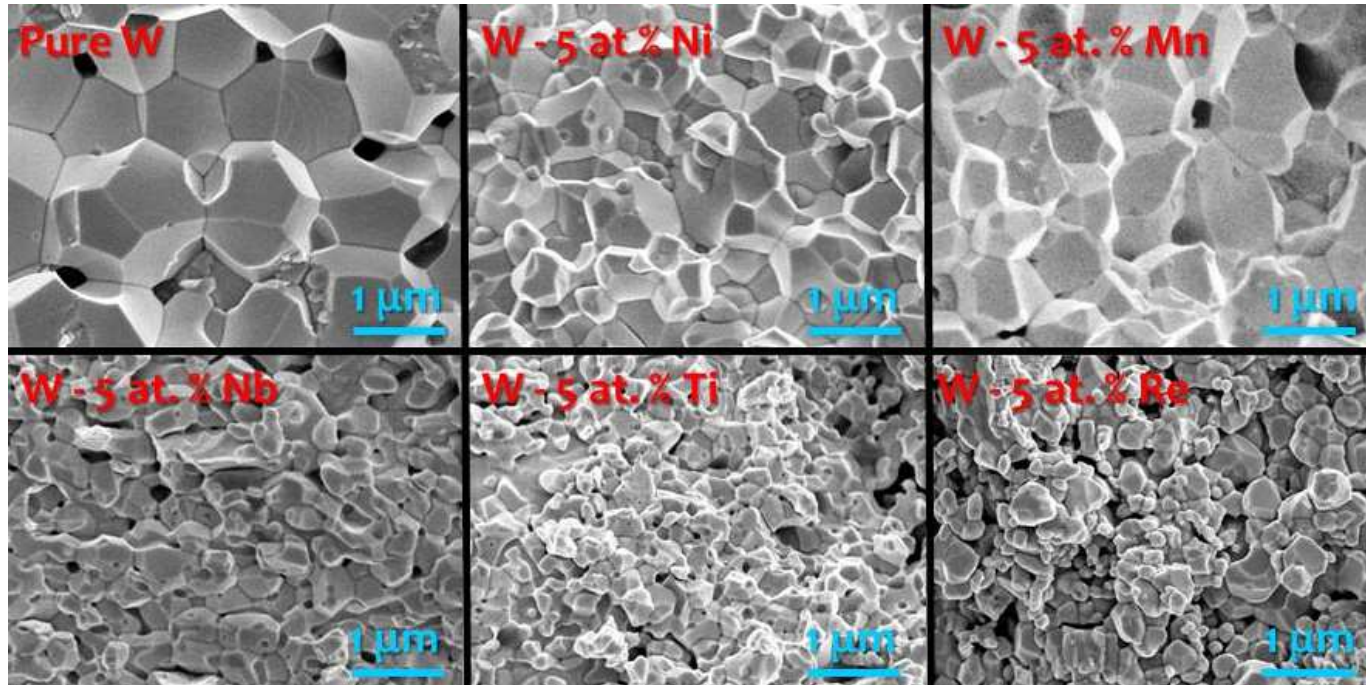
W - 5 at. % Zr (~260 nm)



W - 5 at. % Re (~220 nm)

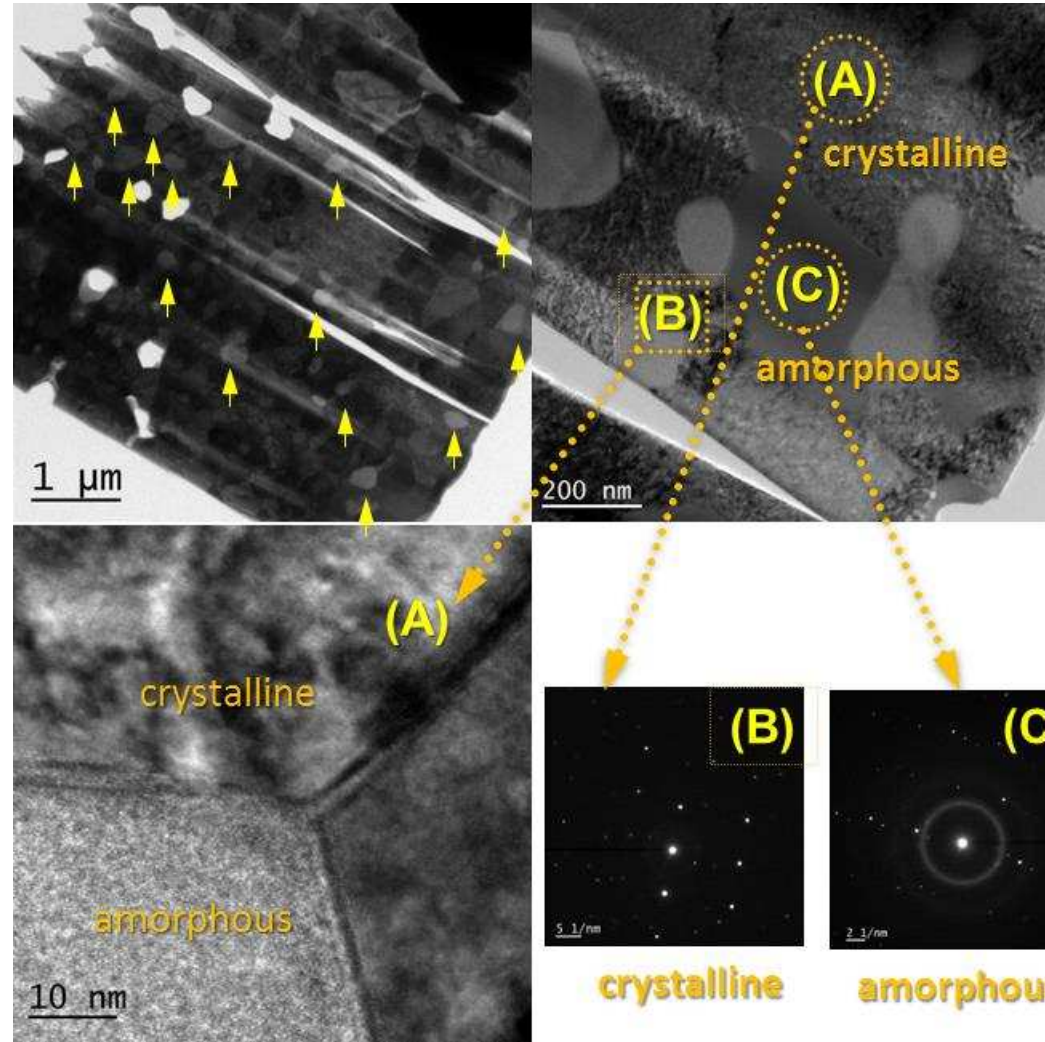
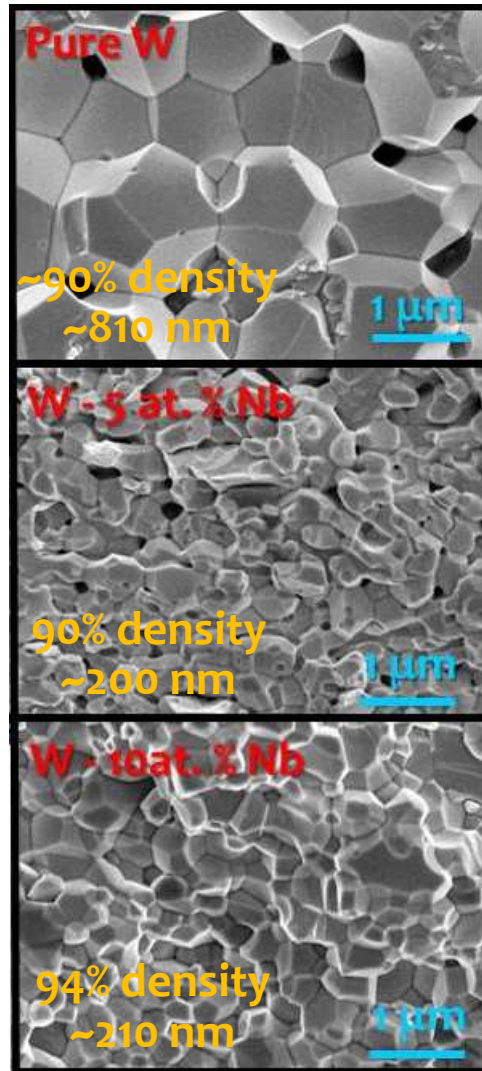


Task 1-B (UCSD):
Spark Plasmas Sintering:
Pure vs. Ni-, Mn-, Nb-, Ti-, and Re-doped W Specimens



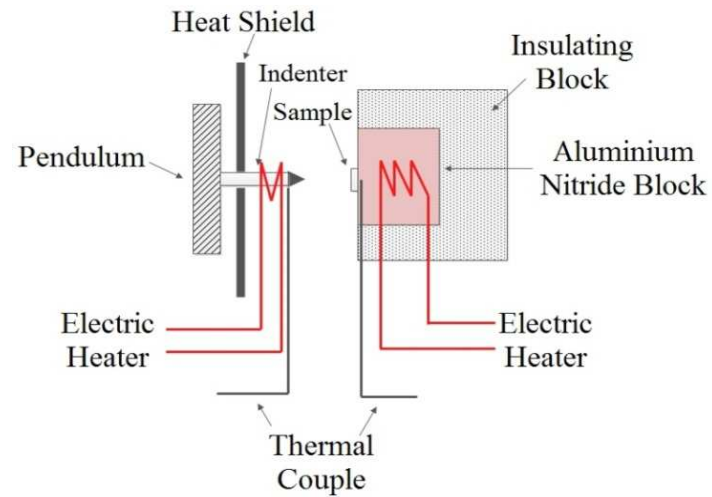
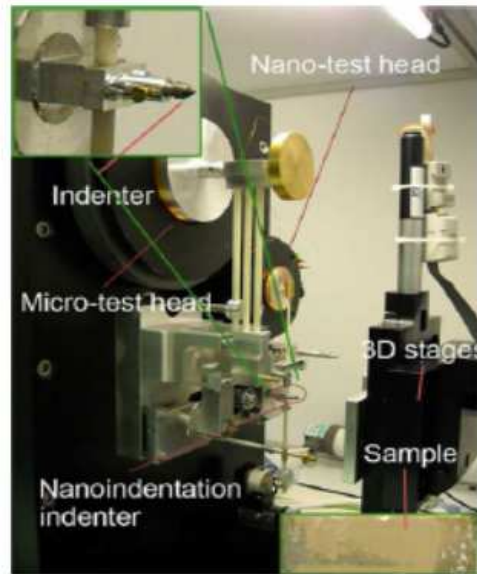
Composition	Relative Density	Grain Size (nm)	Hardness (HRC)
Pure W	90 ± 1%	810 ± 230	42
W – 5 at. % Ni	95%	440 ± 140	49
W – 5 at. % Ti	80%	145 ± 40	42.5
W – 5 at. % Mn	85%	570 ± 200	24.5
W – 5 at. % Re	84%	132 ± 41	33
W – 5 at. % Nb	90%	202 ± 64	44

Task 1-B (UCSD):
TEM Characterization of SPS Specimens (W-Nb)

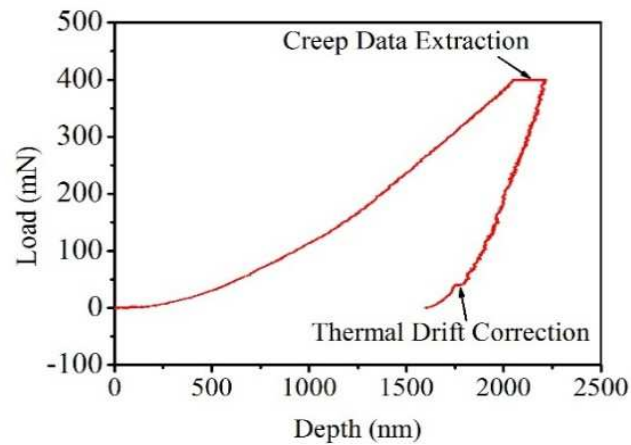


Enhanced Sintering w/ Minimum Grain Growth Attributed to the Formation and Fast Transport in Amorphous Phase in W-Nb Specimens

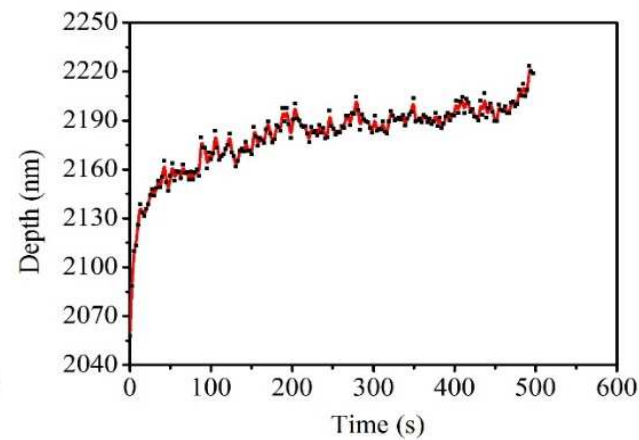
Task 2-High Temperature Nanoindentation Tests



(a.)



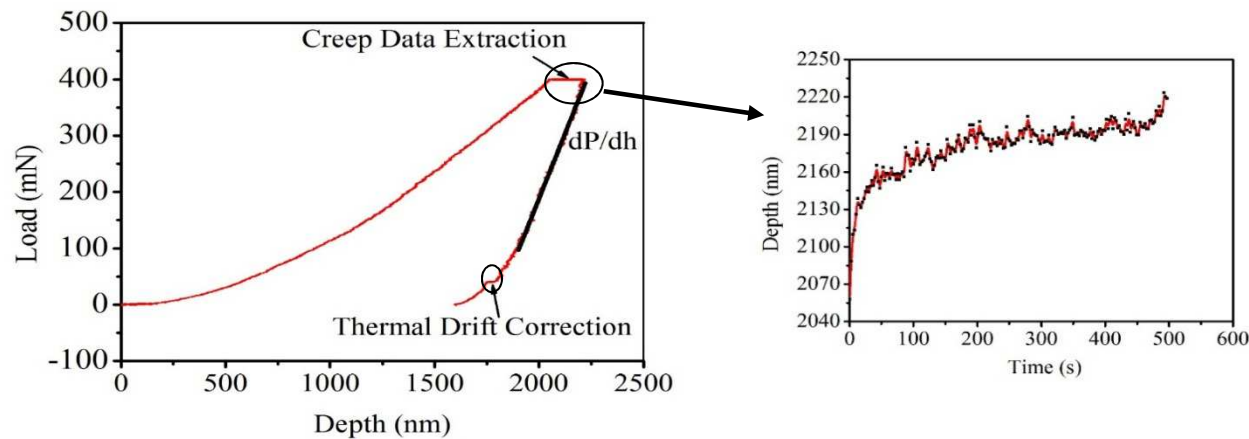
(b.)



(c.)

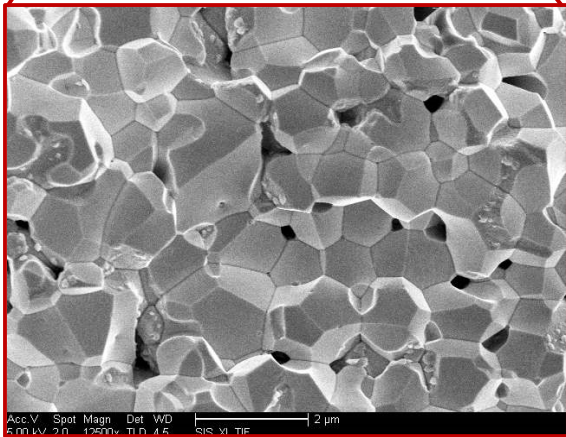
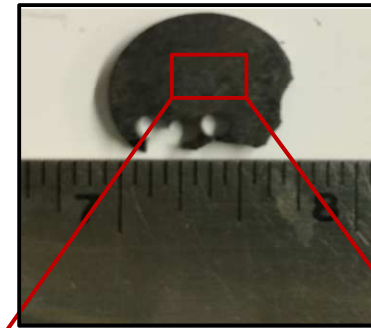
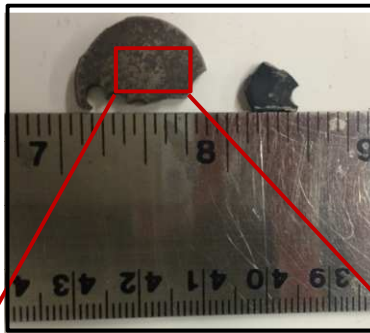
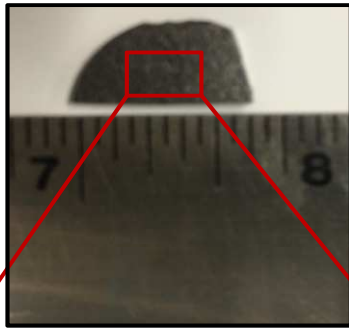
Nanoindentation Creep

- Conventional creep experiments are done on metals with tensile loading
- For small scale materials creep is extracted through nano/micro indentation [Easterling, 1991]
- Impact of creep deformation of the mechanical properties of the materials evaluated [Ngan, 2004]
- Indentation Creep:

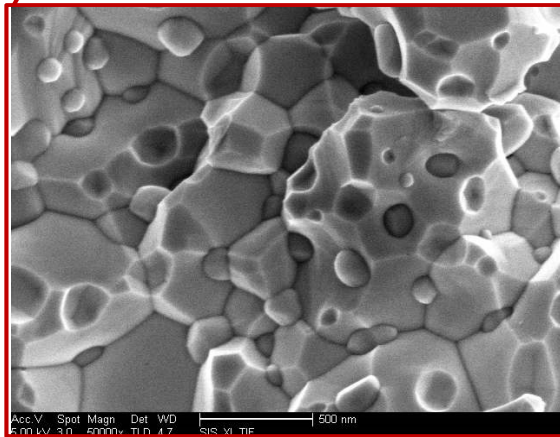


Typical Indentation Curve & Creep Data Extraction
[Zhang, 2015]

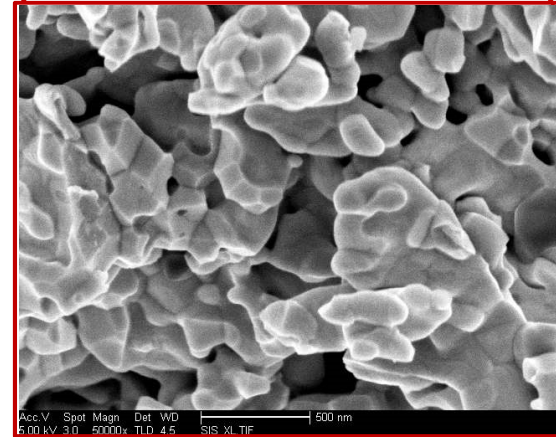
SPS Sample Images



**W Sintered at 1200C
for 5min**

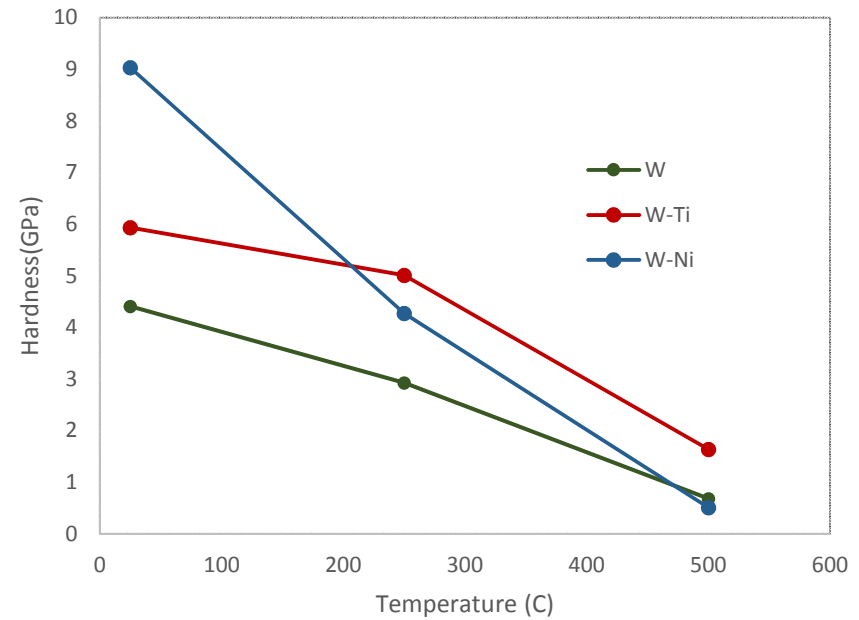
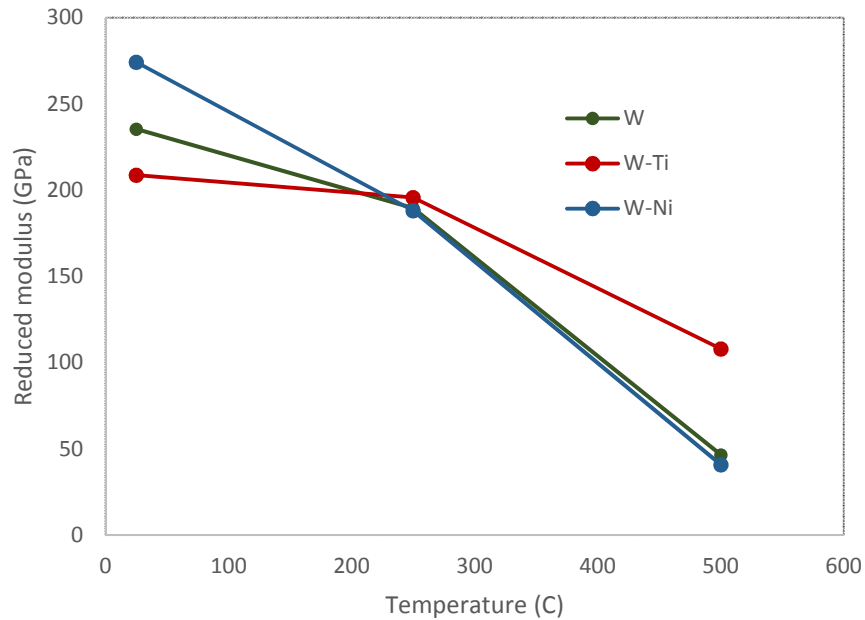


**W-5%Ni Sintered at
1200C for 5min**



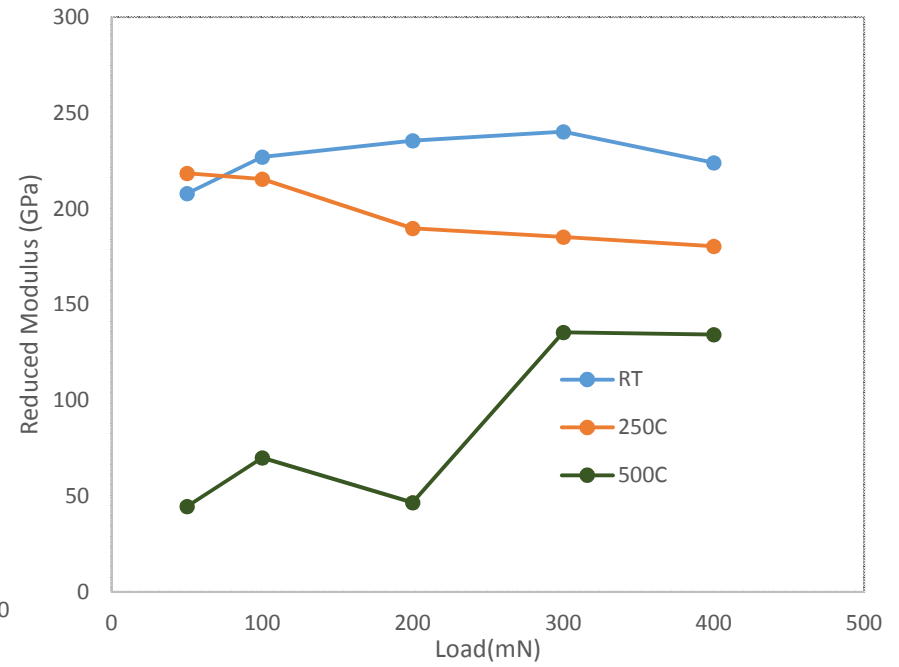
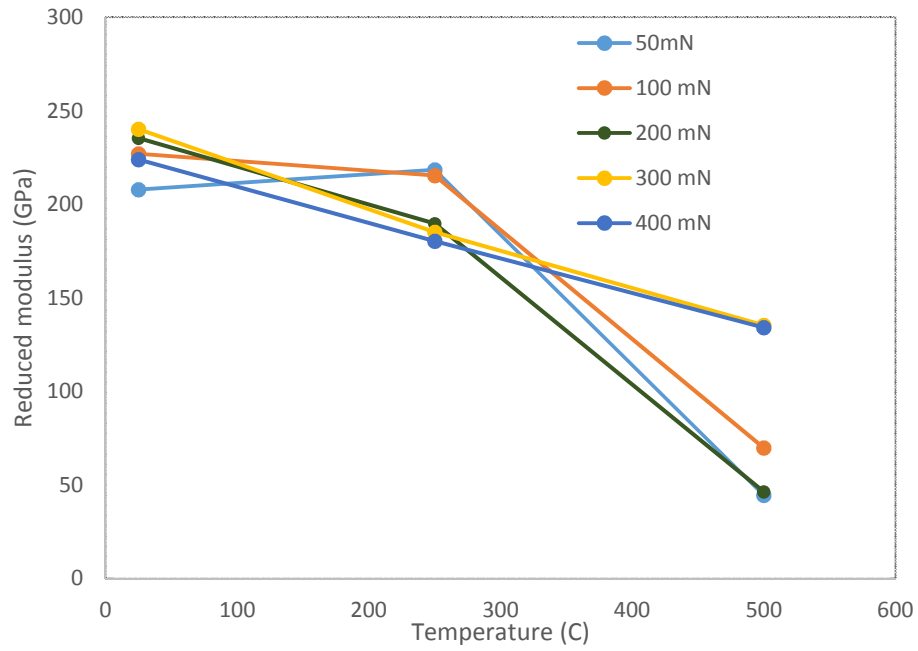
**W-5% Ti Sintered at
1200C for 5min**

Mechanical Properties

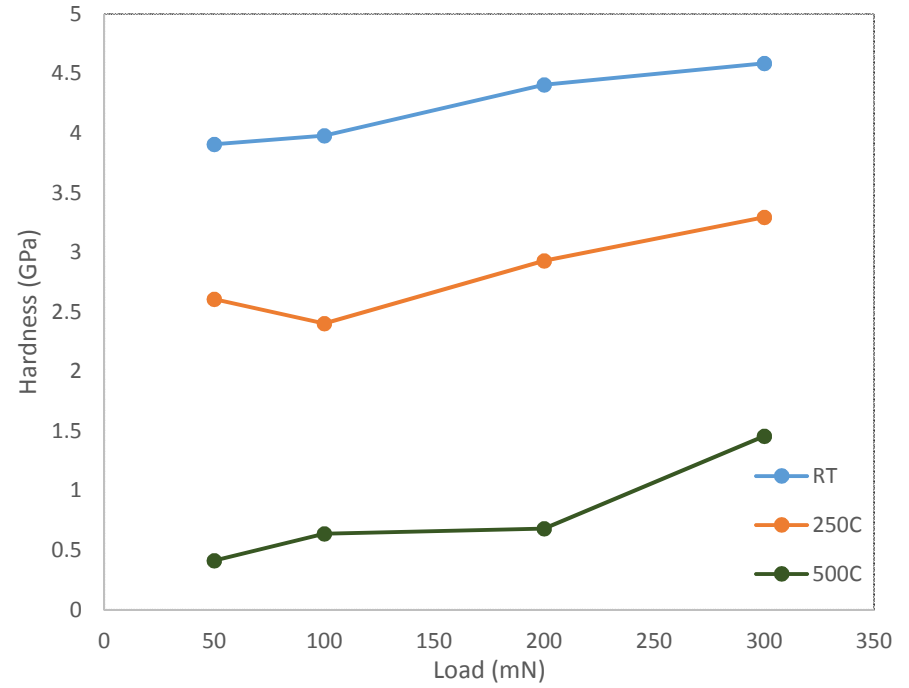
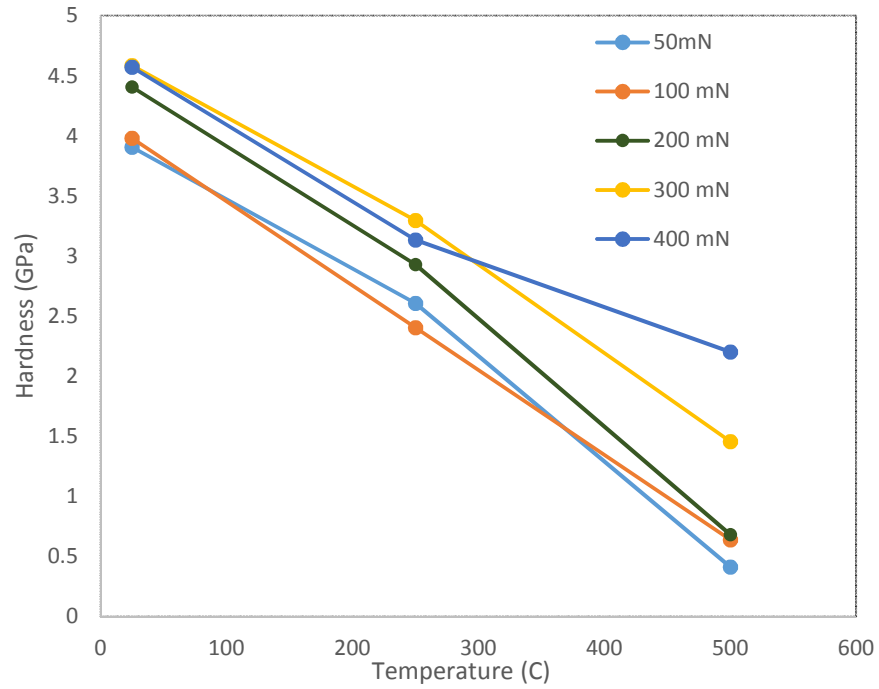


- Hardness and reduced modulus reduces with increase in temperature
- Impurities improve the strength of sintered tungsten

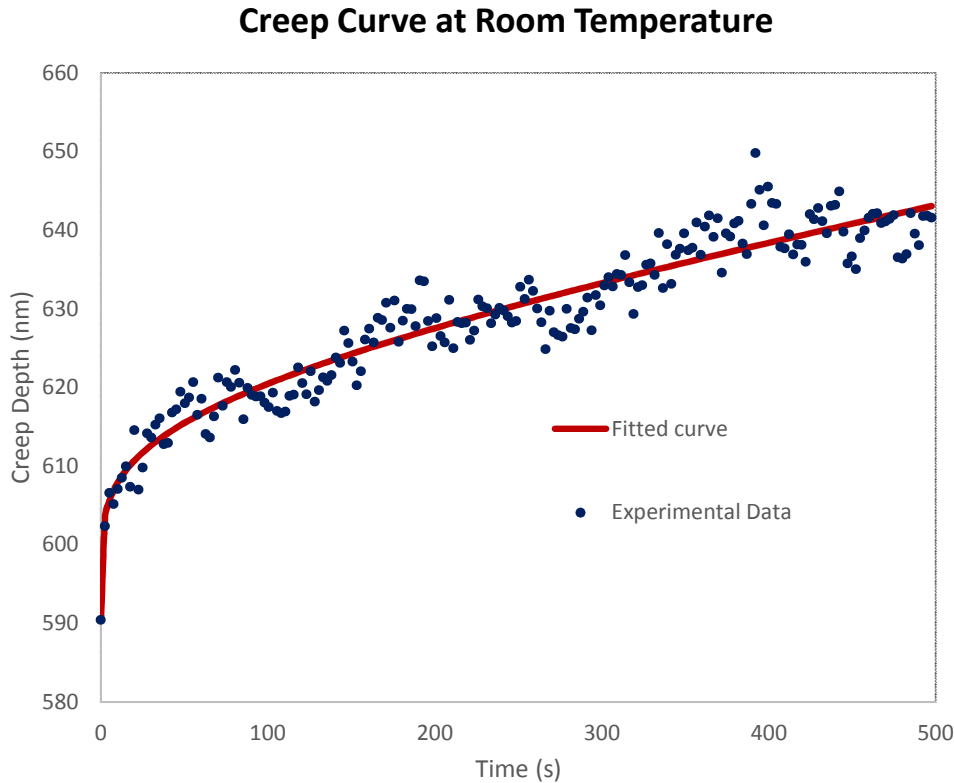
Reduced Modulus (Pure W)



Hardness (Pure W)



Creep Curve



Curve fitted to creep data, $h(t) = h_0 + at^b + kt$
Fitting constants are tabulated below,

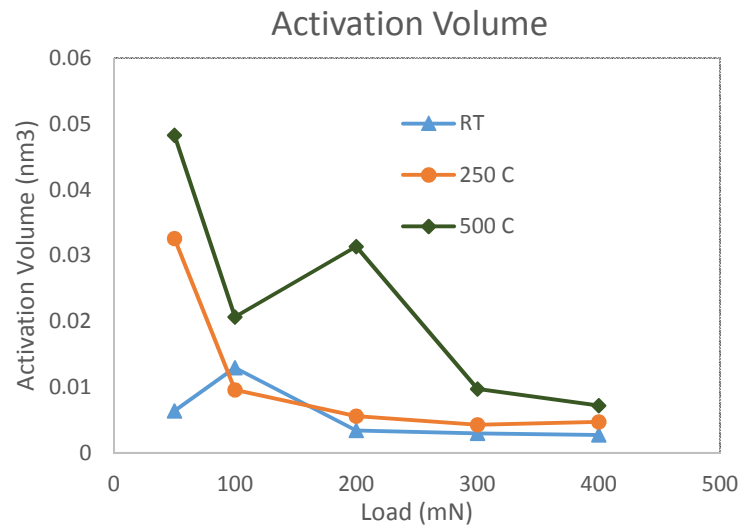
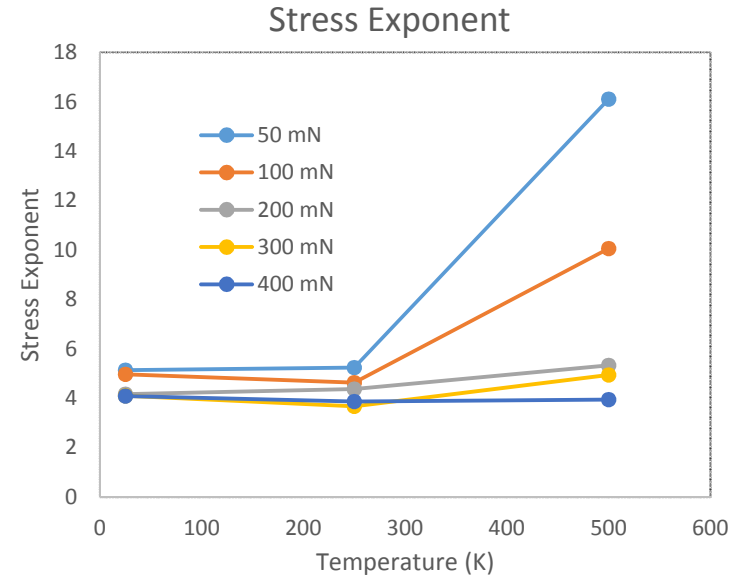
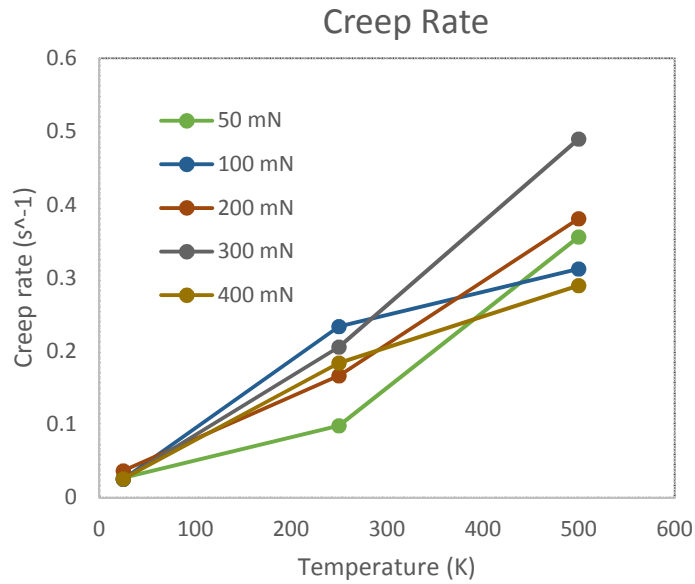
a	11.7876
h0	589.4798
b	0.185692
k	0.032633
Max Load	50 mN

$$\text{Stress Exponent, } n = \frac{\ln(\dot{\epsilon})}{\ln(\sigma)}$$

$$\text{where } \dot{\epsilon} = \frac{1}{h(t)} \frac{dh}{dt} \text{ and } \sigma = \frac{P_{\max}}{A}$$

with general area function, $A = 18.72h_c^2 + 11542.71h_c$

Creep Properties (Pure W)



Task 3 (UCSD):

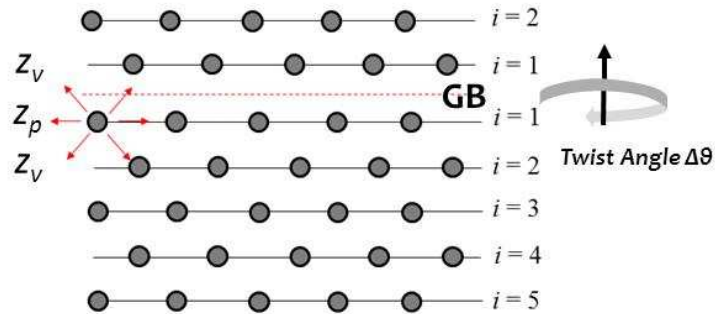
A New Theoretical Framework to Characterize GB Segregation

- **Task 3-A:** The Classical GB Segregation Model: Assessments of W alloys w/ the Wynblatt-Chatain Model & Construction of GB Adsorption Diagrams
- **Task 3-B:** Non-Classical High-T GB Segregation (Coupled w/ Interfacial Disordering) → Construction of “GB λ diagrams” for W-based Binary Alloys
- **Task 3-C:** Predicting GB Diffusivity Maps from Computed “GB λ diagrams” + Limited Experimental Data (The Newest Advancement & Future Direction)

Task 3-A: Classical GB Segregation/Adsorption Model

Assessment of W Alloys by the Wynblatt-Chatain Model → (New) GB Adsorption Diagrams

Key Assumption/Simplification: No GB Premelting/Interfacial Disordering



A McLean Type Segregation Equation

$$\frac{X_i}{1 - X_i} = \frac{X_\infty}{1 - X_\infty} \exp\left(-\frac{\Delta H_i^{seg}}{kT}\right)$$

i -th Layer Composition

Bulk Composition

Segregation Enthalpy:

$$\Delta H_i^{seg} = \begin{cases} \underbrace{-0.5Q(e_{BB} - e_{AA})z_v}_{\text{Bonding-Energy Difference}} + \underbrace{\Delta E_{el}^i}_{\text{Strain Energy}} + \underbrace{2\omega_S}_{\text{Interactions}} \begin{bmatrix} zX_\infty - z_pX_1 - z_vX_2 \\ -(1-Q)z_vX_1 - \frac{1}{2}Qz_v \end{bmatrix} & i=1 \\ \underbrace{-\Delta E_{el}^i}_{\text{Strain Energy}} + \underbrace{2\omega_S}_{\text{Interactions}} (zX_\infty - z_pX_i - z_vX_{i+1} - z_vX_{i-1}) & i>1 \end{cases}$$

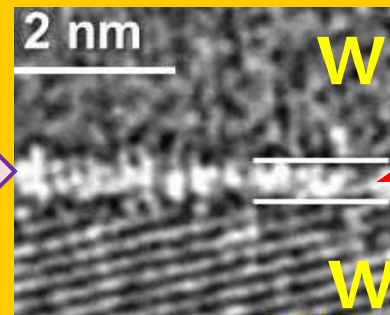
GB Absorption: $\Gamma_{GB} = 2 \sum_i (X_i - X_\infty)$



Complimentary to the Model to Forecast High-T Interfacial Disordering (Discussed in Task 3-B)

A “New” Type of High-T (Premelting-Like) GB Segregation

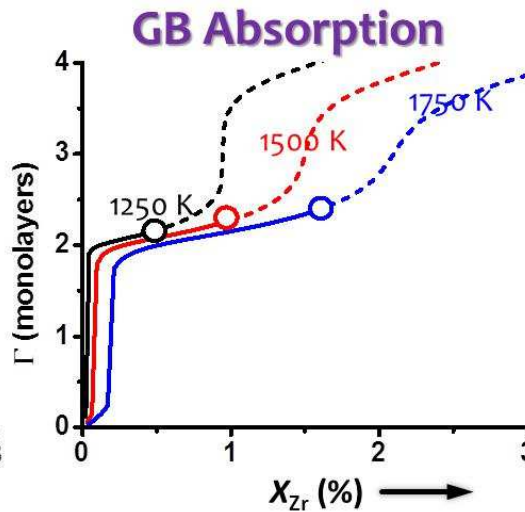
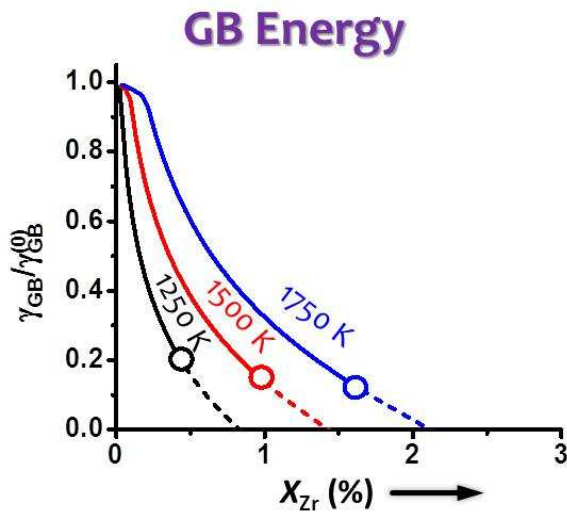
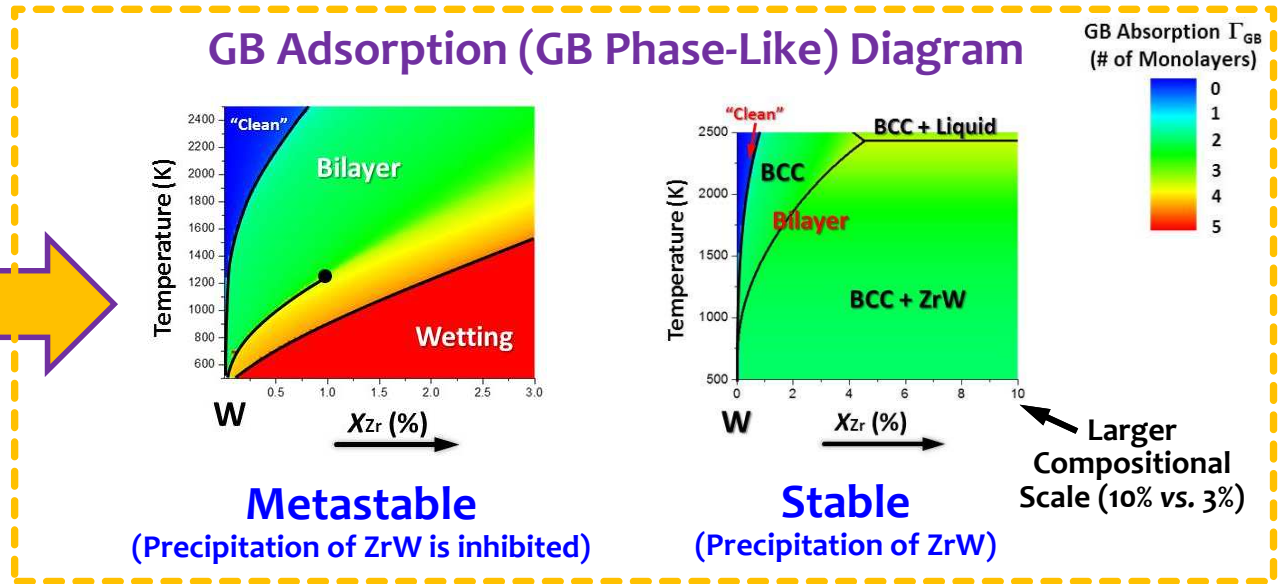
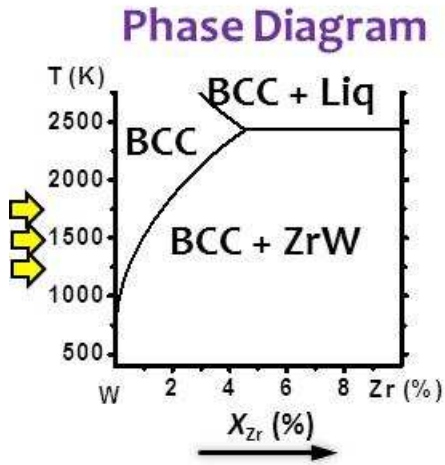
Discovered and modeled by Luo et al. at Clemson/UCSD



Impurity/Dopant-Based Quasi-Liquid Interfacial “Phase” @ $T < T_{solidus}$

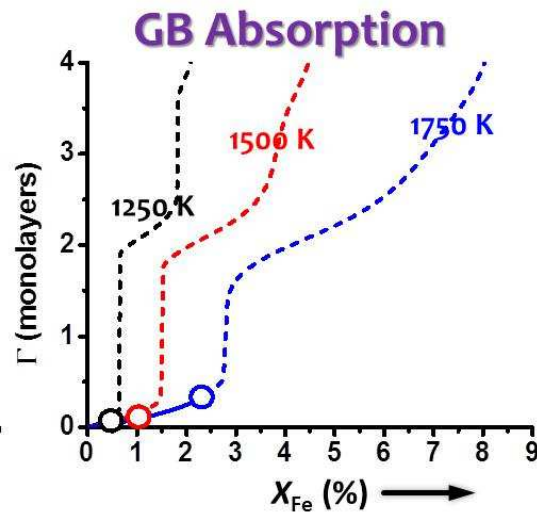
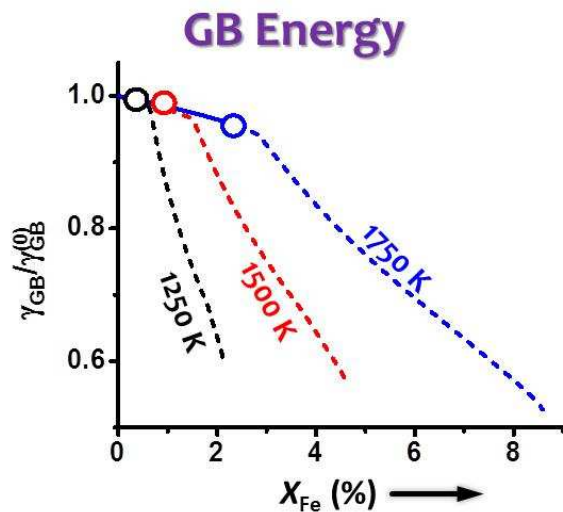
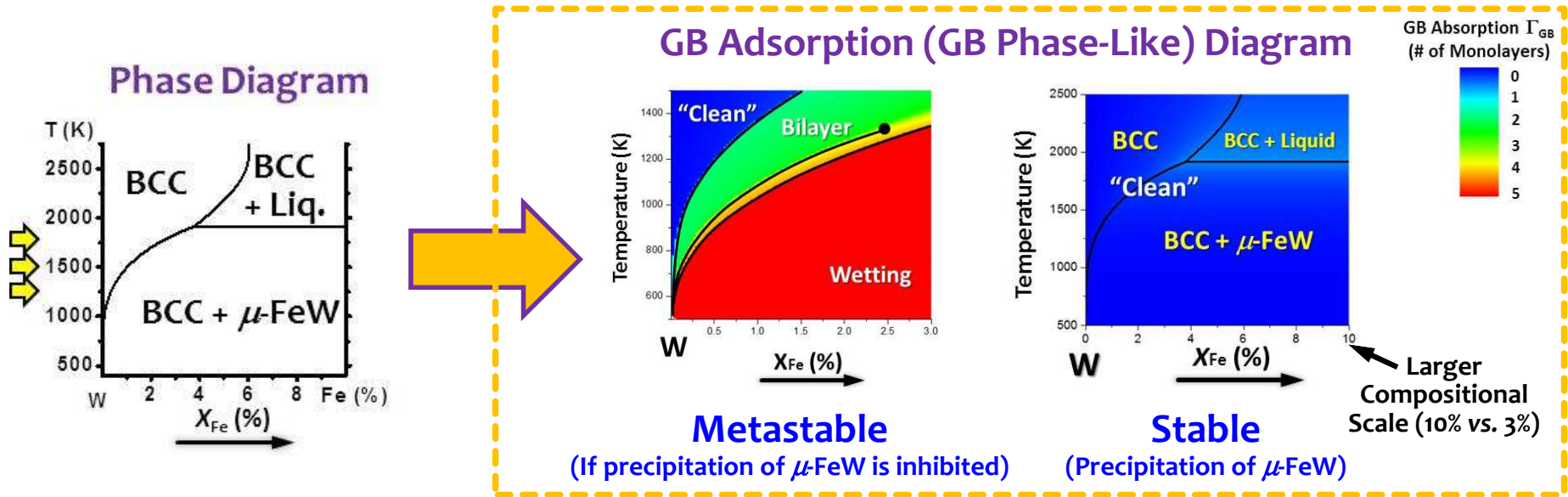
Task 3-A (UCSD): Classical GB Segregation (No GB Premelting/Disordering) Example #1

GB Adsorption & Transitions in W-Zr



Task 3-A (UCSD): Classical GB Segregation (No GB Premelting/Disordering) Example #2

GB Adsorption & Transitions in W-Fe

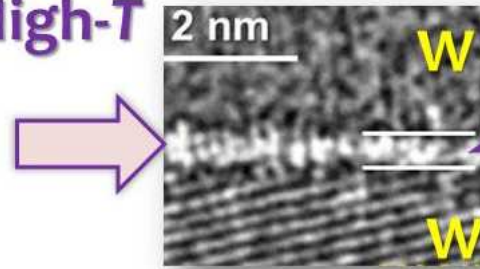


No Classical GB Adsorption Transition @Equilibrium!

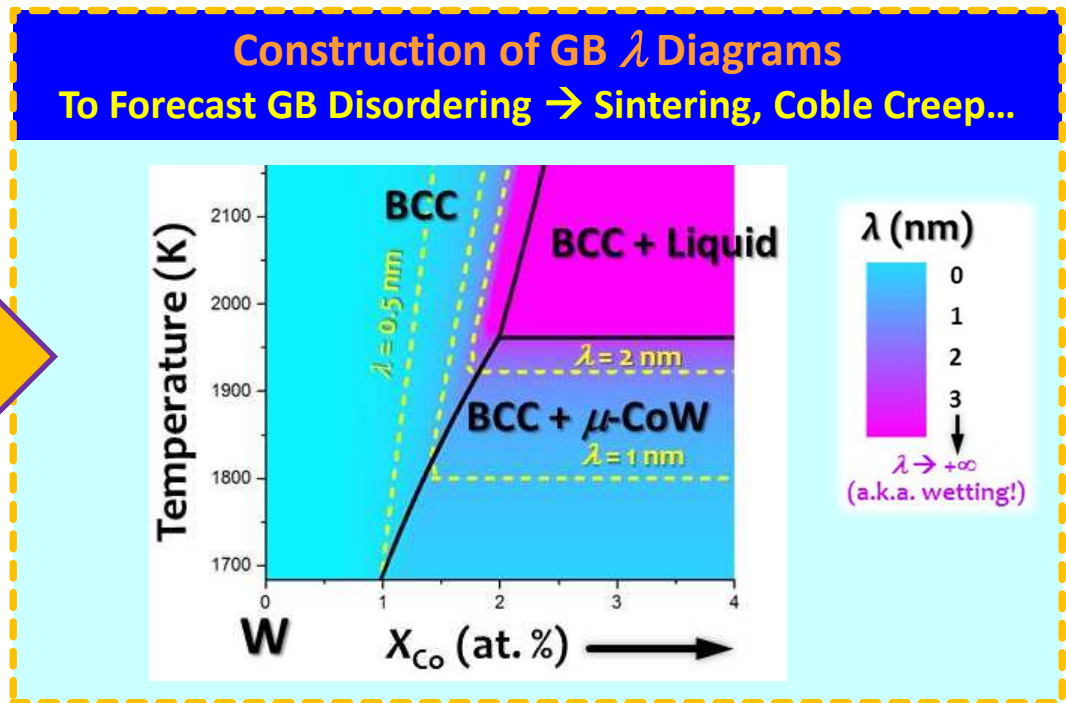
(a.k.a., classical GB adsorption transitions only occur when the precipitation of μ -FeW is kinetically inhibited)

Task 3-B: High-T Segregation + GB Disordering

A “New” Type of High-T
(Premelting-Like)
GB Segregation
Discovered and modeled by
Luo et al. at Clemson/UCSD



Impurity/Dopant-
Based Quasi-Liquid
Interfacial “Phase”
@ $T < T_{\text{solidus}}$



A Thermodynamic Variable: λ
Luo & Shi, Appl. Phys. Lett. 92:101901 (2008)

Thermodynamically stable if:
 $\Delta G_{\text{amorph.}} \cdot h < -\Delta\gamma$

Define & quantify:
 $\lambda \equiv \text{Max}_{(0 < X_M < 1)} \left\{ \frac{-\Delta\gamma}{\Delta G_{\text{vol}}} \right\}$

Representing the thermodynamic tendency to stabilize a quasi-liquid film

λ scales the film thickness
Continuum approx. for metals:
 $f(h) \approx 1 - e^{-h/\xi}$ (Coherent length)
 $h_{\text{BQ}} \approx \xi \cdot \ln(\lambda / \xi)$

Miedema type “macroscopic atom” model
(Benedictus-Böttger-Mittemeijer Model)
 $\gamma_{\alpha} = F_M^W(X_M) \cdot \frac{\Delta H_{\text{interface}}^{W/M}}{C_0 V^{2/3}} + \frac{H_W^{\text{int}}}{C_0 V^{2/3}} + \frac{1.9RT}{C_0 V^{2/3}}$
Benedictus, Böttger, Mittemeijer, Phys. Rev. 54:9109 (1996)
A recent review: Jurgens, Wang, Mittemeijer, Int. J. Mat. Rev. 100:211 (2009)

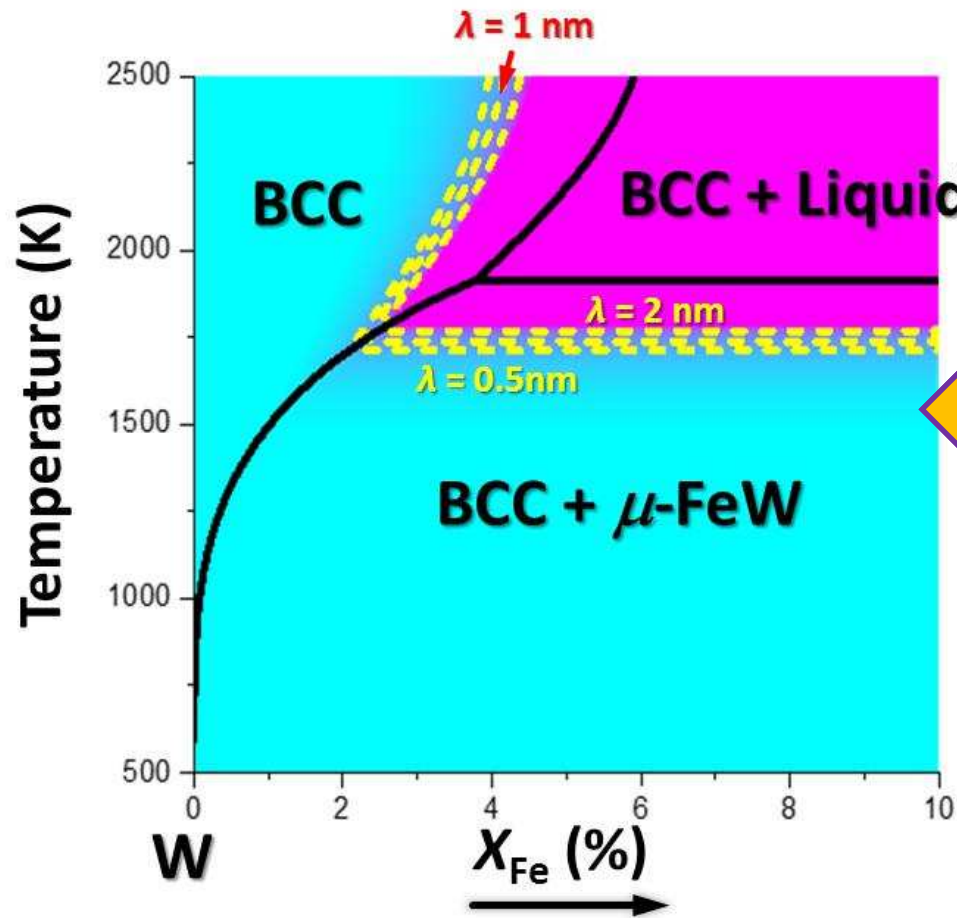
CalPhaD
 $\Delta G_{\text{vol}} = G_{\text{liquid}}^f - [X_M \mu_M + (1 - X_M) \mu_W]$

Thermodynamic Functions (for W-Pd, W-Ni, W-Co, W-Fe):
Guillet, Metall. Trans. A 1980;
Gustafson, Metall. Trans. A, 1987;
Gustafson, Z. Metallkd. 1988;
Gustafson, et al. Z. Metallkd. 1987; Lee et al., Calphad 1986.

How does this Task 3-B support our overall project goal (of modeling creep)?

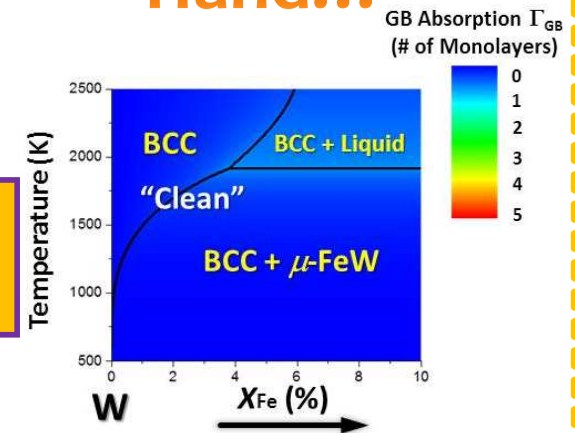
- \rightarrow “GB λ Diagram” + Limited Experiments \rightarrow GB Diffusivity Map (Task 3-C at UCSD)
- \rightarrow Multiscale modeling of microstructure-dependent Coble creep (Task 4 at Purdue)

Task 3-B (UCSD): High-T Segregation + GB Disordering Example #1
Computed GB λ Diagram for W-Fe



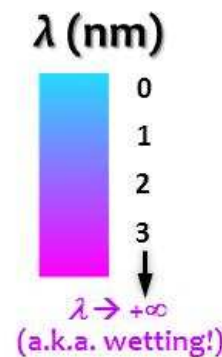
GB Disorder More Important!

On the Other Hand...



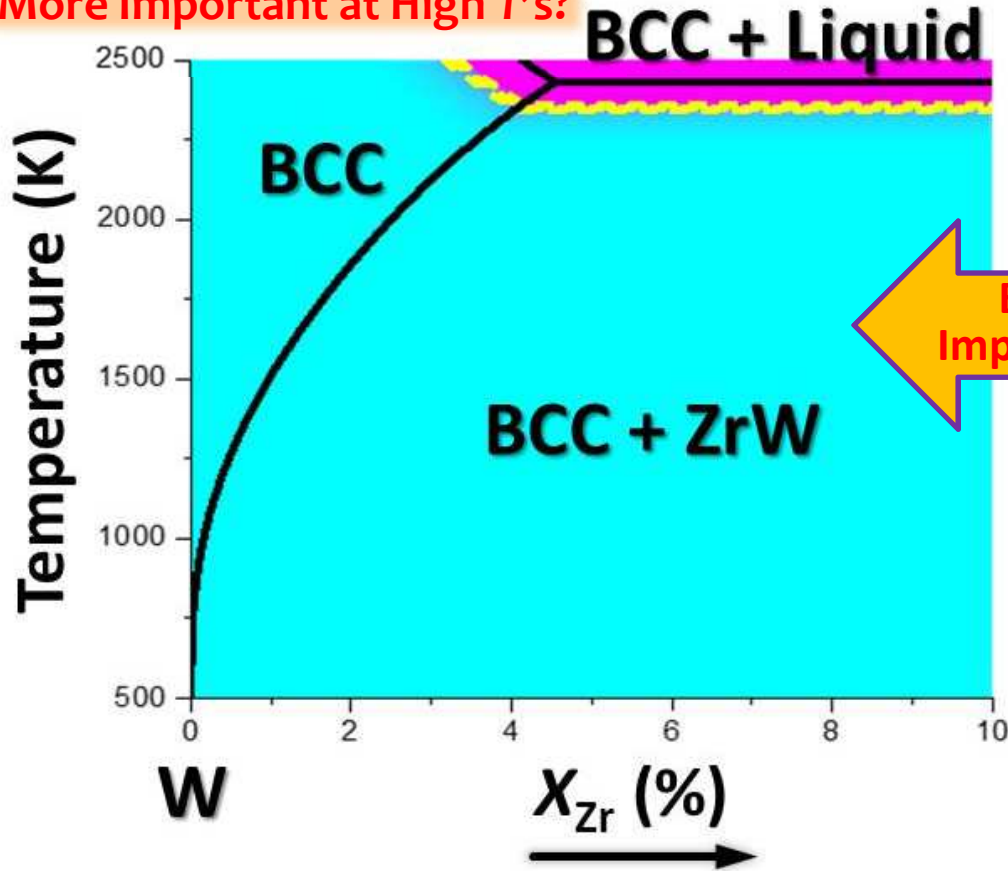
No Classical GB Adsorption Transition @ Equilibrium!

Premelting-Induced High-T Segregation Dominant!



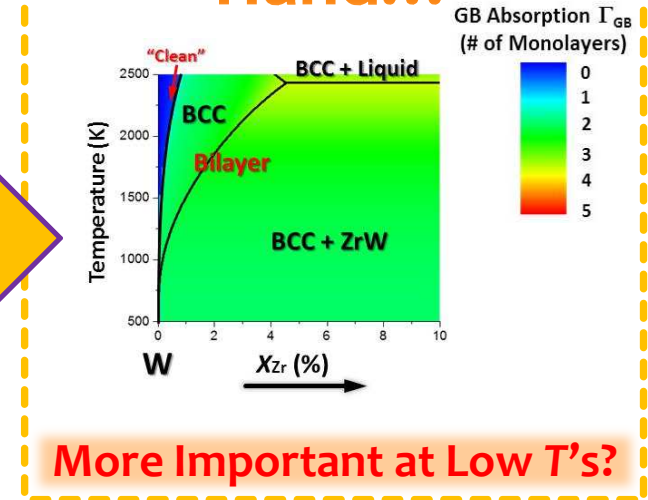
Task 3-B (UCSD): High-T Segregation + GB Disordering Example #2
Computed GB λ Diagram for W-Zr

More Important at High T 's?



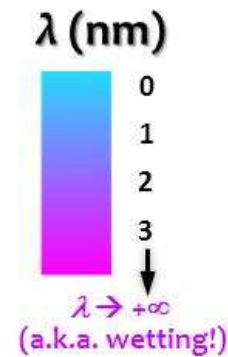
Both Important!

On the Other Hand...



More Important at Low T 's?

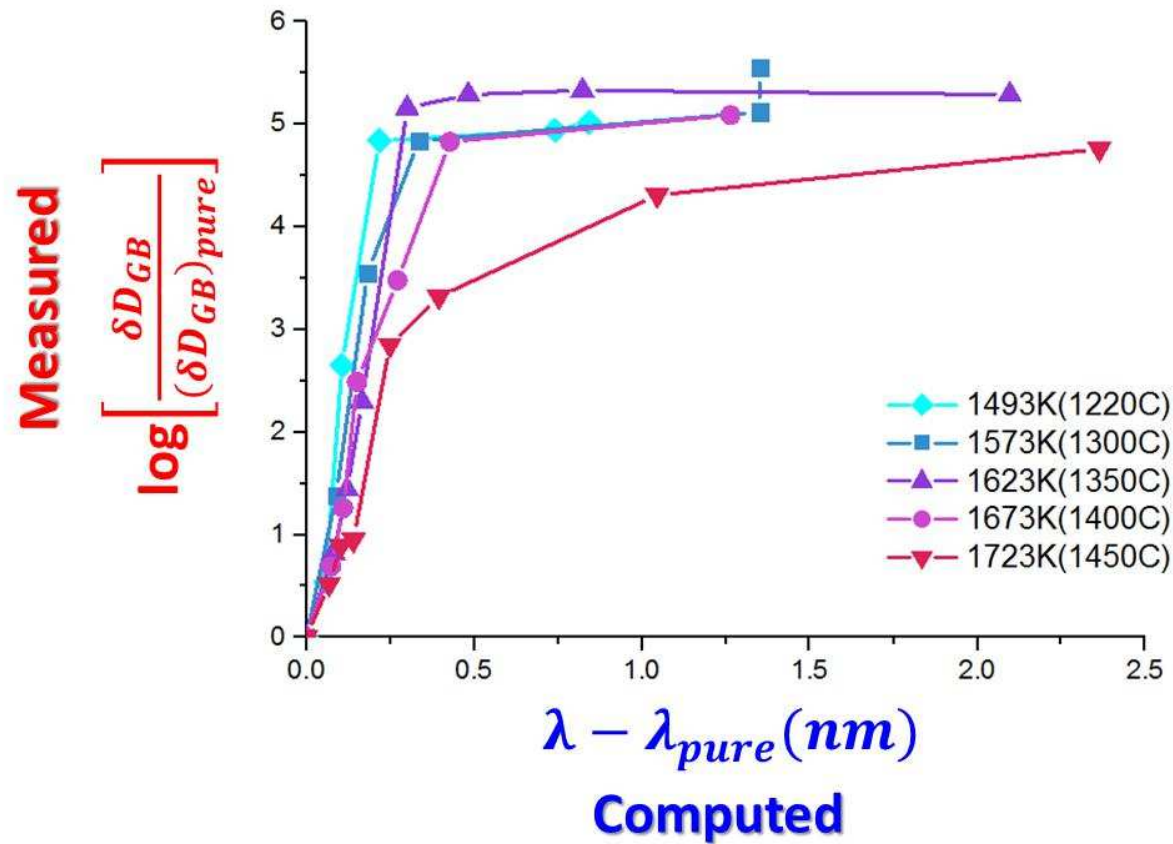
Both Types of GB Segregation Important!



Task 3-C: Can we predict GB Diffusivity Maps from Computed GB λ Diagrams?

Correlation: Computed λ 's vs. Measured GB Diffusivities

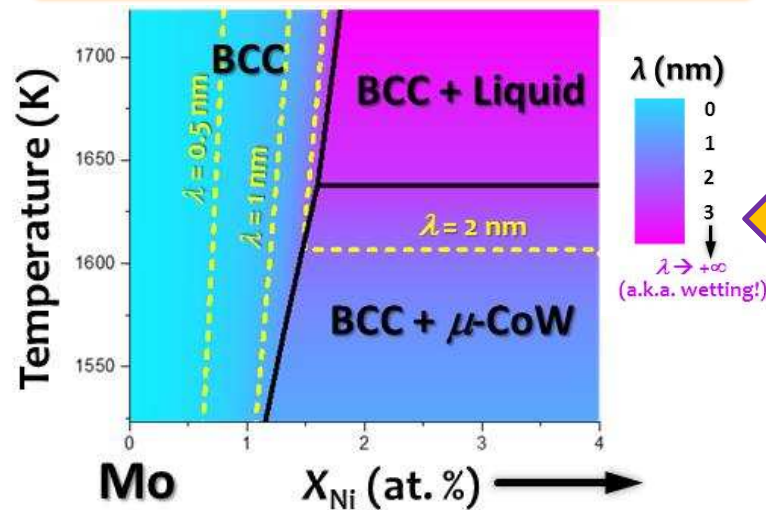
Learning from the Mo-Ni System...



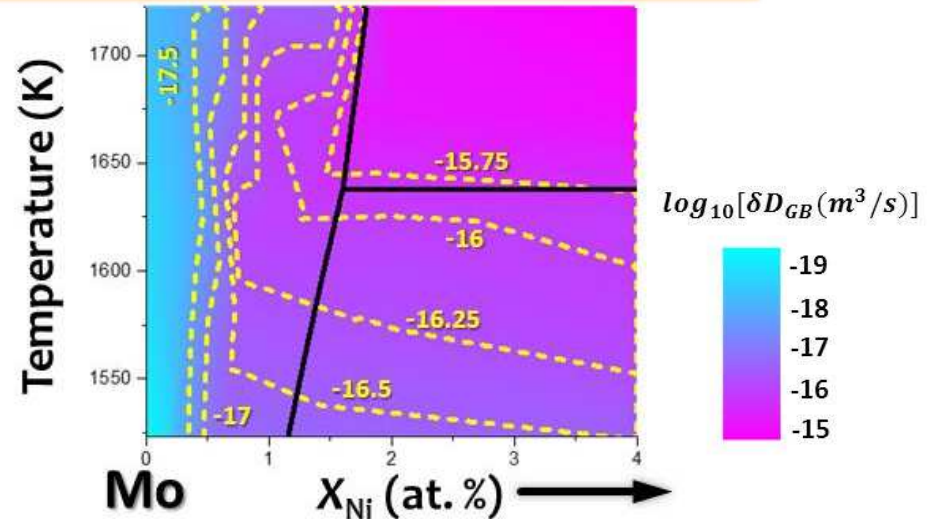
$$\ln \left[\frac{\delta D_{GB}}{(\delta D_{GB})_{pure}} \right] = 4.958 * \left\{ 1 - \exp \left[- \left(\frac{\lambda - \lambda_{pure}}{0.1928} \right)^2 \right] \right\}$$

Task 3-C: Predicting GB Diffusivity Maps from Computed GB λ Diagrams” Learning from Mo-Ni : Successfully Reproducing the GB Diffusivity Map

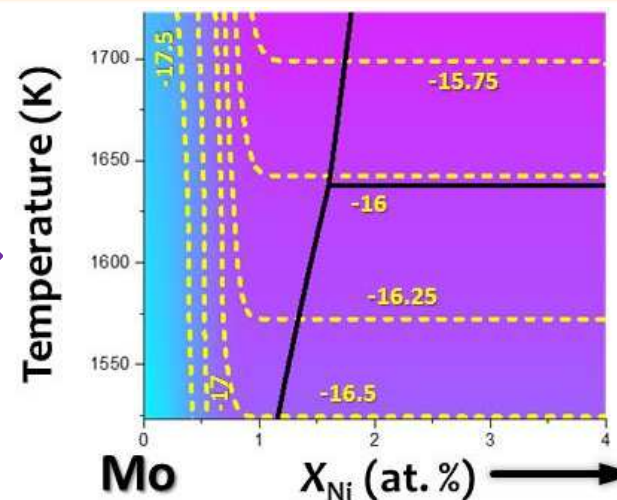
Mo-Ni: Computed GB λ Diagram



Mo-Ni: Measured GB Diffusivity Map



Mo-Ni: Calculated GB Diffusivity Map



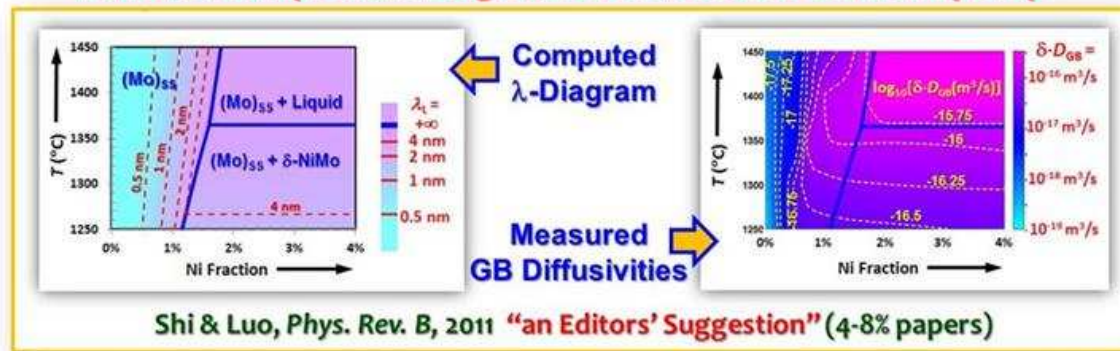
**Forecasting?
 Successfully
 Reproduced!**

$$\ln \left[\frac{\delta D_{GB}}{(\delta D_{GB})_{pure}} \right] = 4.958 * \left\{ 1 - \exp \left[- \left(\frac{\lambda - \lambda_{pure}}{0.1928} \right)^2 \right] \right\}$$

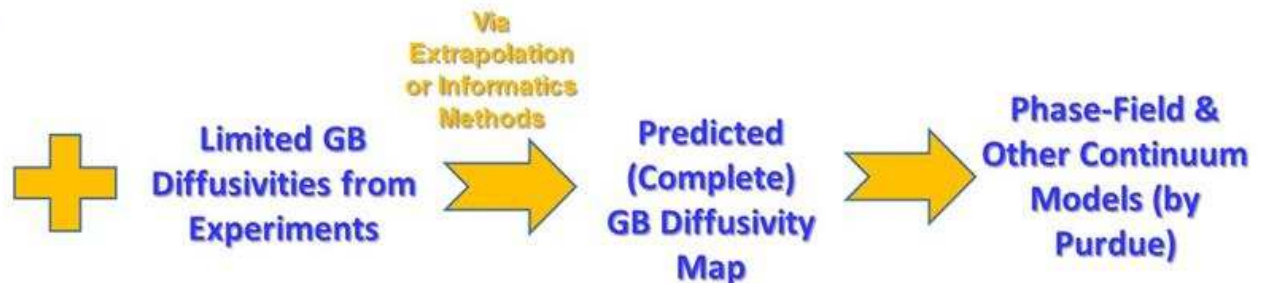
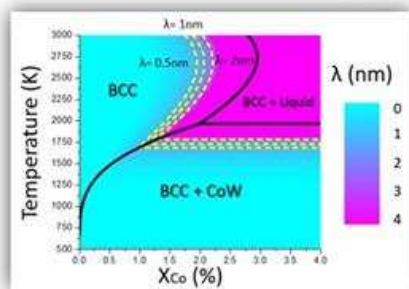
Task 3-C: Predicting GB Diffusivity Maps from Computed “GB λ diagrams” + Limited Experimental Data

(The Newest Advancement & Future Direction)

Learning System: Systematic Correlation
Between Computed λ -Diagram & Measured GB Diffusivity Map



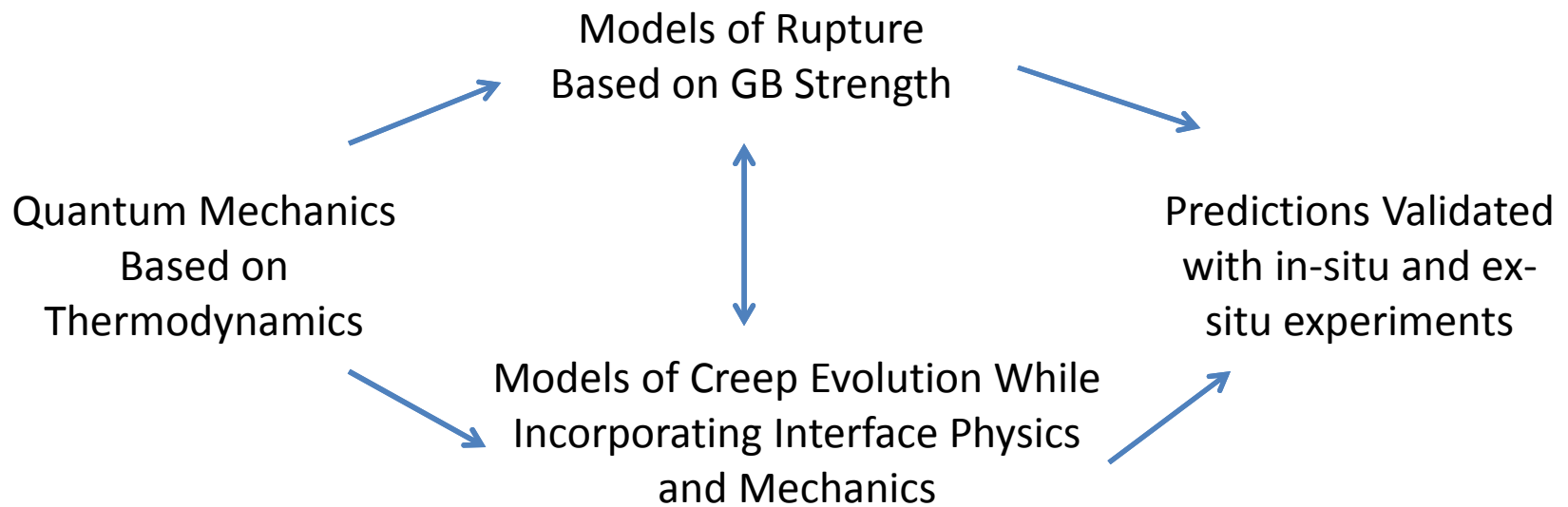
A New Computed λ -diagram



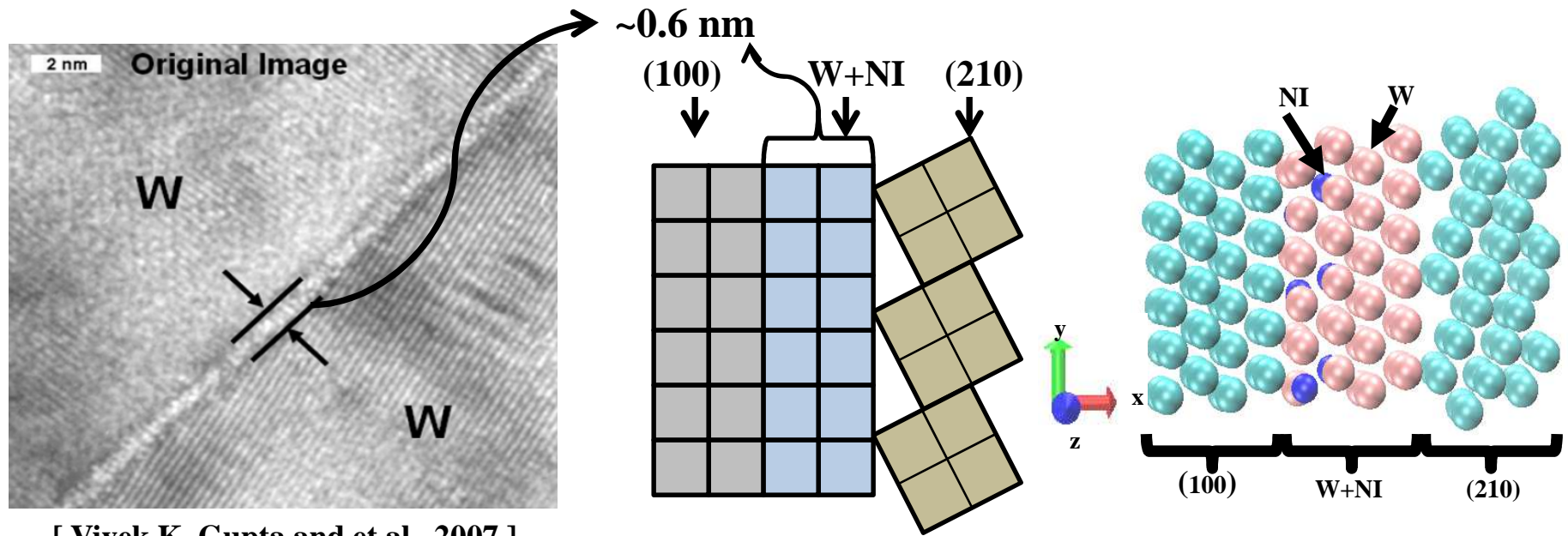
On-Going/Future Studies (A High-Risk Thrust)...

- To forecast GB diffusivity maps for W based binary alloys & validate the predictions
- To support multiscale modeling of Coble creep at Purdue

Task 4: Multiscale Models for Rupture Strength and Long Term Creep



➤ Quantum mechanical calculation of GB Strength

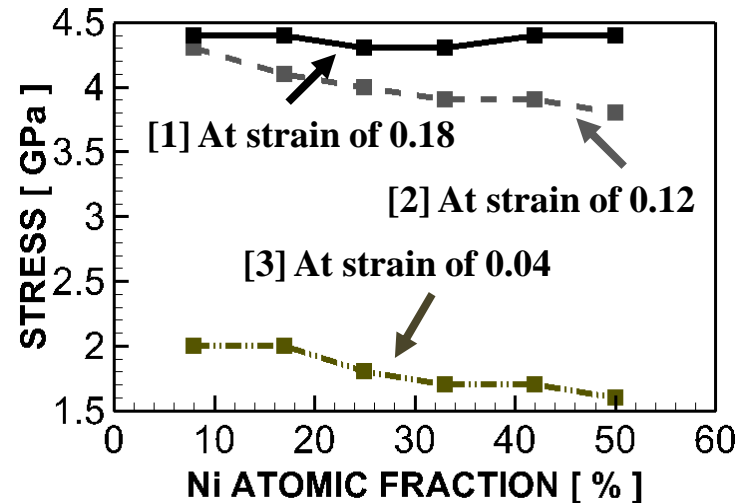
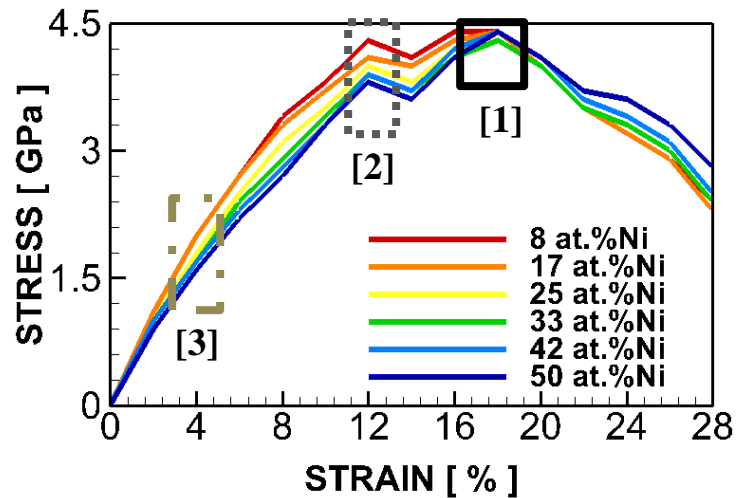


[Vivek K. Gupta and et al., 2007]

- ❖ time step: 5 a.u. , total 2000 steps Becquart and et al., 2006
- ❖ cutoff energy for wavefunction : 350 eV Nose and Shuichi, 1984
- ❖ Nose-Hoover thermostat : 300K, 400K, 500K, 600K Hoover and William, 1985
- ❖ electronic fake mass for CPMD : 400 a.u. Perdew and et al., 1996 Vanderbilt and David, 1990
- ❖ number of k-points for integration over Brillouin zone : 32x32x32 Monkhorst and Pack., 1996

➤ Stress – strain relation

(1) Unsaturated Ni - W



Yield strength: at strain 4%,

First peak: at strain 12%

Yield strength and first peak's values have dependent on the Ni volume fraction.

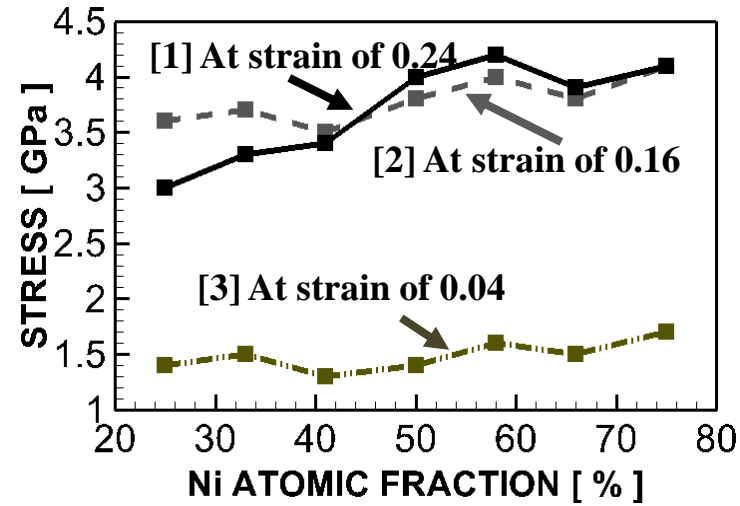
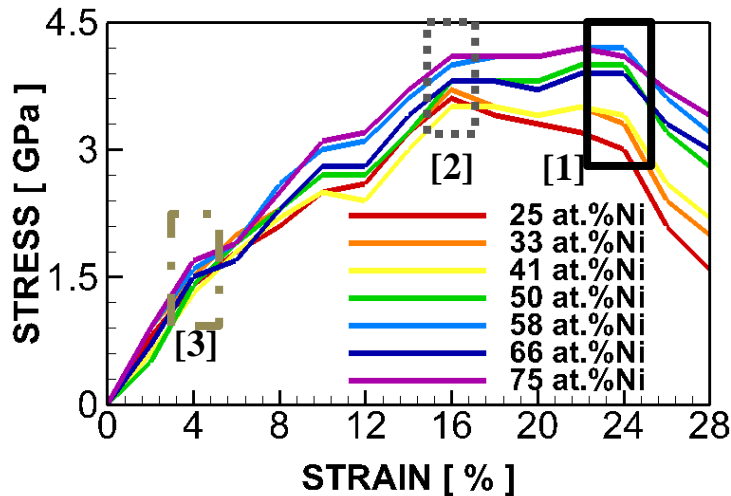
Second peak: at strain 18%

The second peak's values are not depend on the Ni volume fraction.

Ultimate tensile strength : strain of 12~18%

The maximum tensile strength is not affected by Ni volume fraction for the unsaturated W-Ni.

(2) Saturated Ni - W



Yield strength: at strain 4%,

First peak: at strain 16%

Yield strength and first peak's values have dependent on the Ni volume fraction.

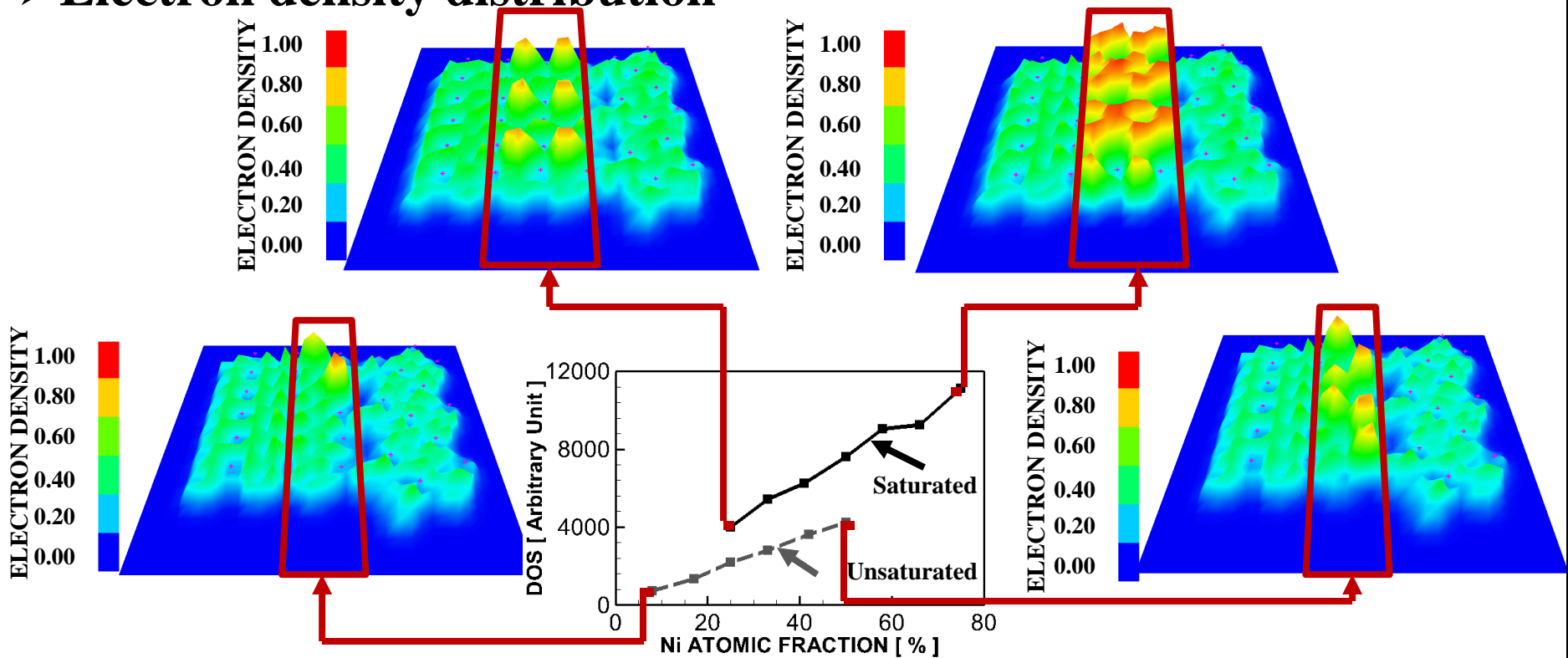
Second peak: at strain 24%

The second peak's values have the largest dependence on the Ni volume fraction.

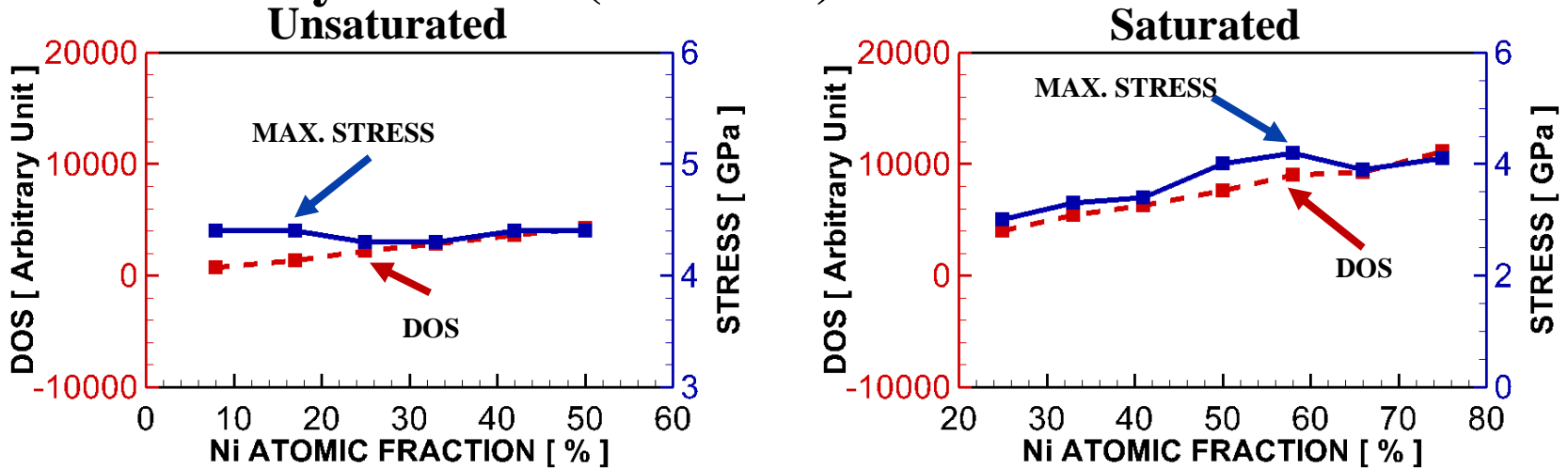
Ultimate tensile strength : strain of 16~24%

The maximum tensile strength is not affected by Ni volume fraction for the saturated W-Ni.

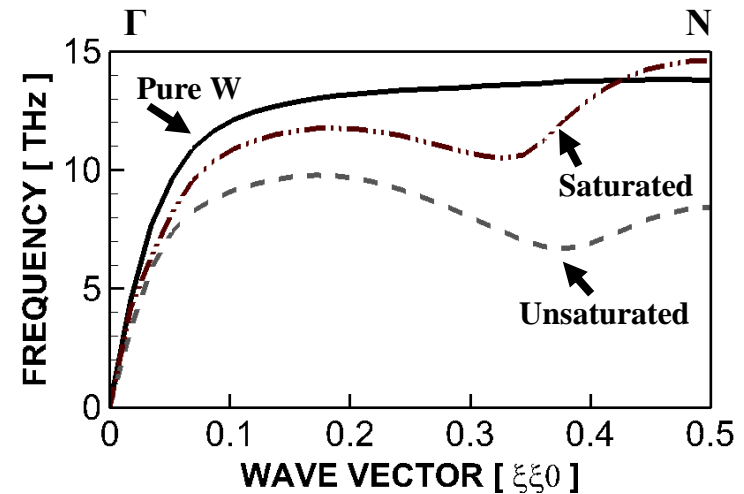
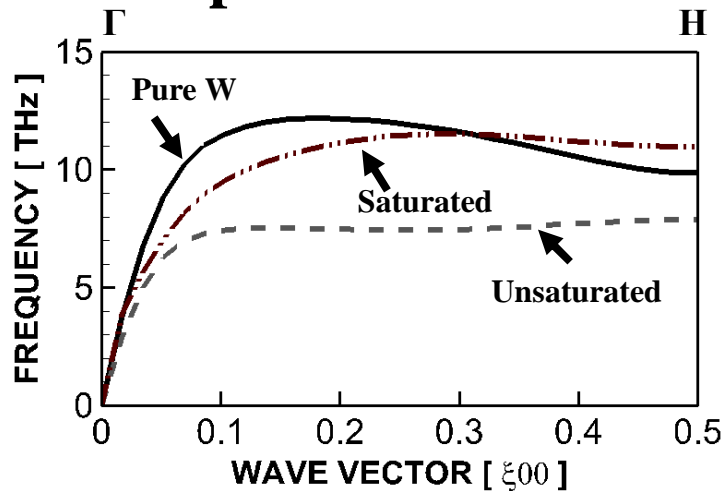
➤ Electron density distribution



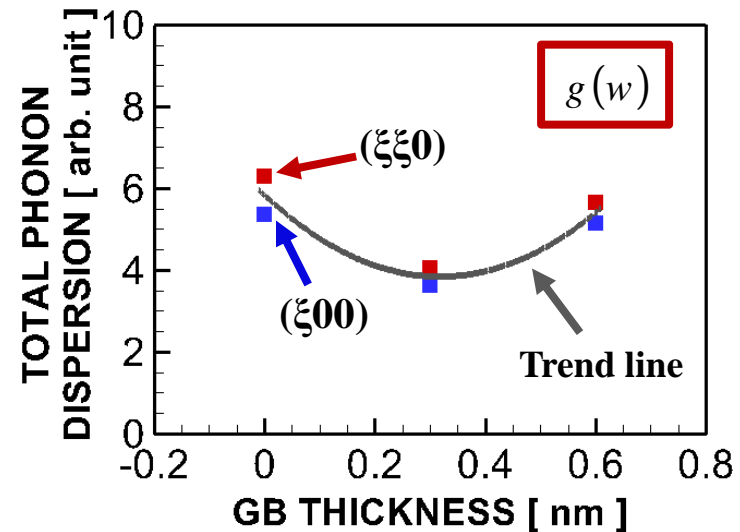
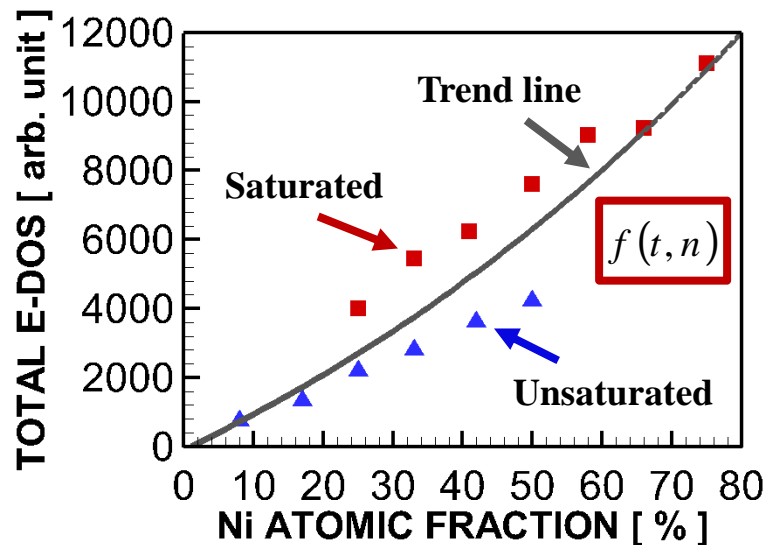
➤ Electron density of states (f-orbital)



➤ Phonon dispersion



➤ Prediction of peak tensile strength



$$\frac{T_{\max}}{T_{\text{ideal}}} = \frac{CE}{CD} \cdot \frac{1}{\Phi} \cdot f(t, n) \cdot g(w)$$

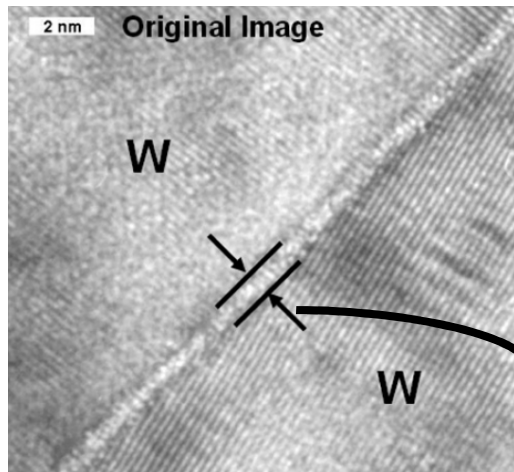
- T_{\max} : Maximum tensile strength of W-Ni alloy
- T_{ideal} : Idealistic maximum tensile strength of W
- Φ : Surface energy of W
- CE : Atomic level cohesive energy of W

How does this prediction apply to continuum scale fracture?

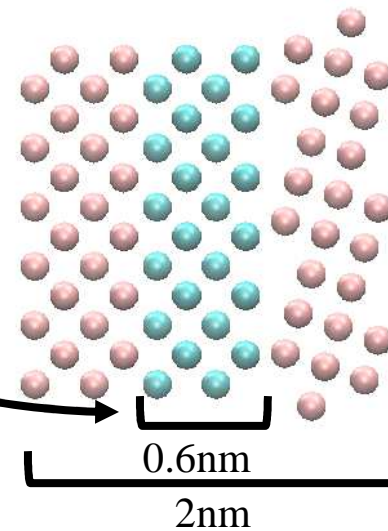


➤ Continuum scale model

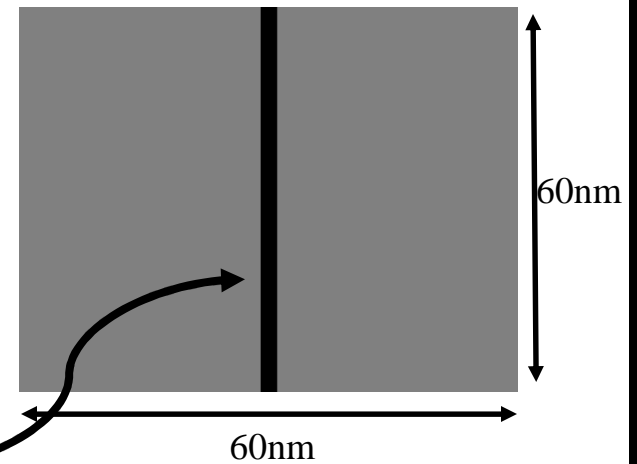
(1) Nano-scale model



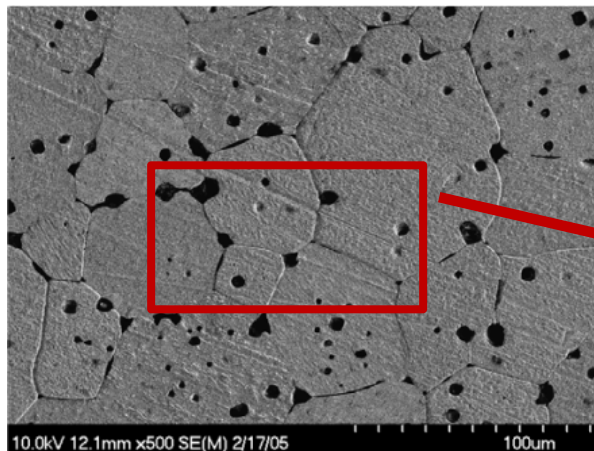
[V. Gupta et al, 2007]



Bi-granular model

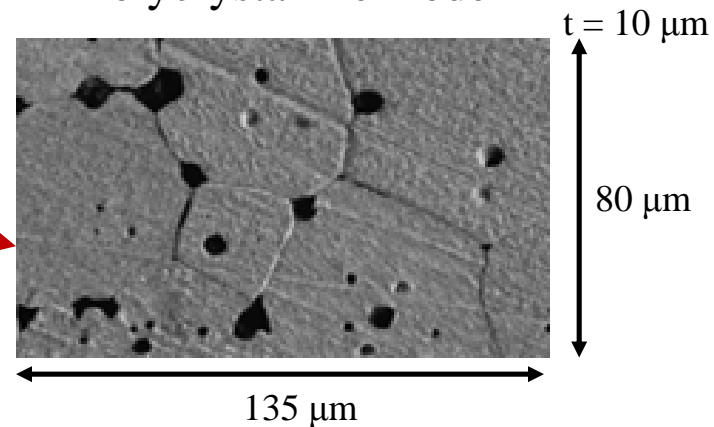


(2) Micro-scale model



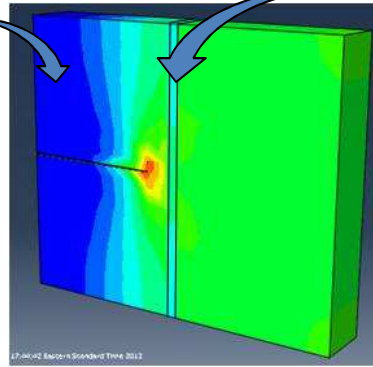
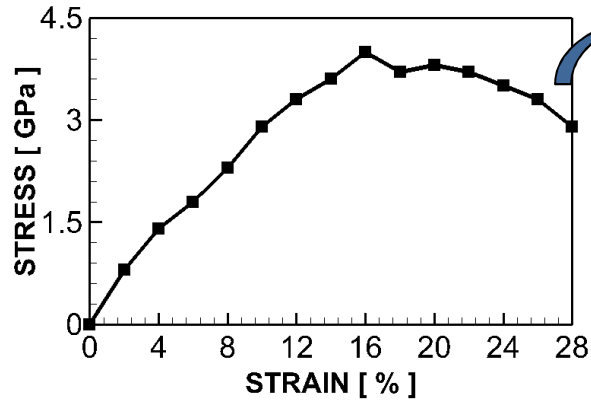
[V. Gupta et al, 2007]

Polycrystalline model

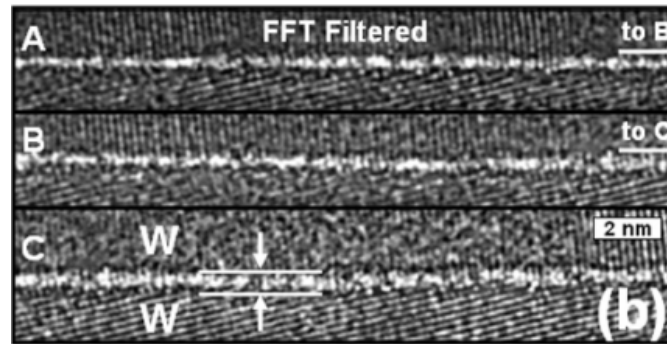
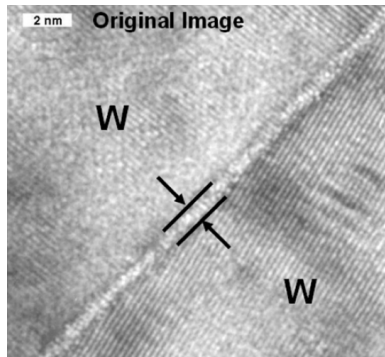
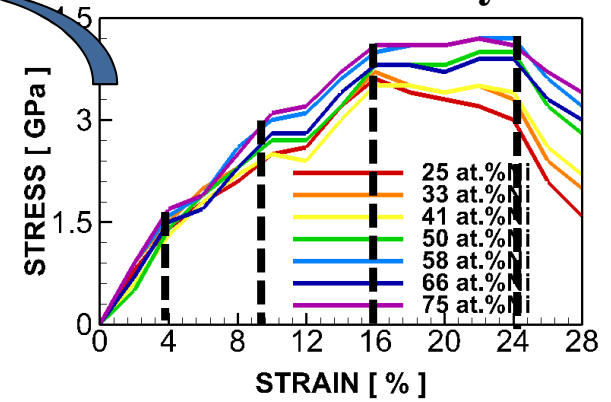


➤ Material model of grains and GBs

Grain

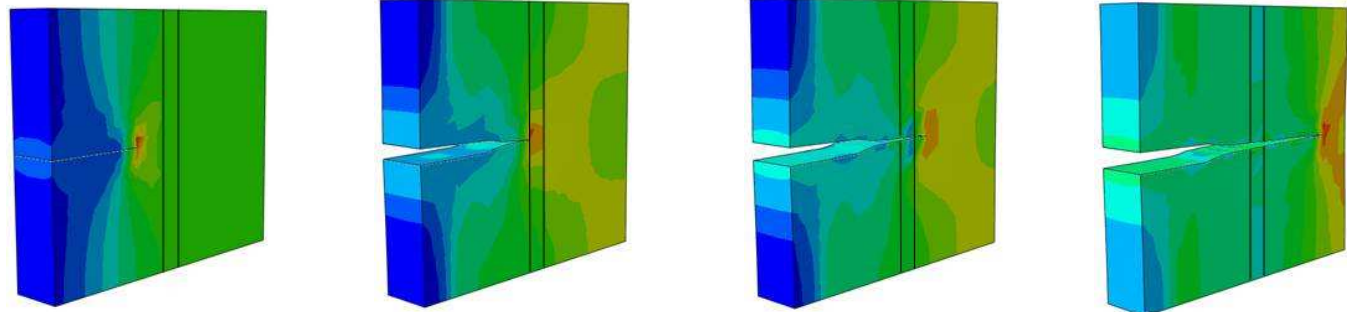


Grain boundary



[V. Gupta et al, 2007]

Crack propagation of GB



Time-step increment

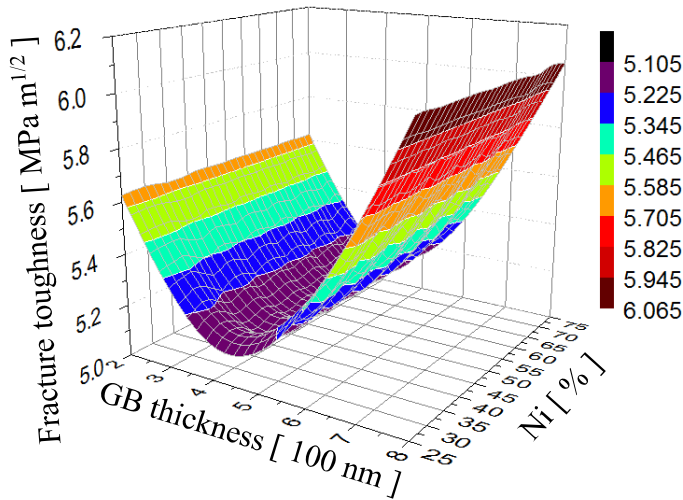
4.5E-5

0.013

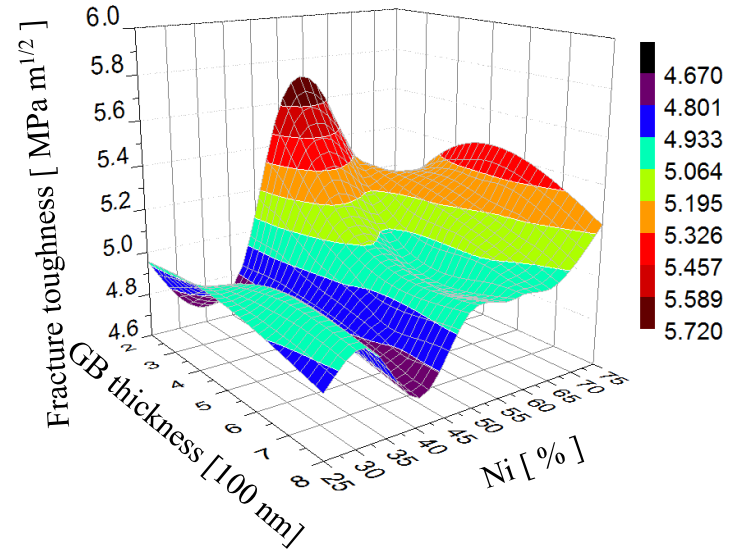
0.015

0.018

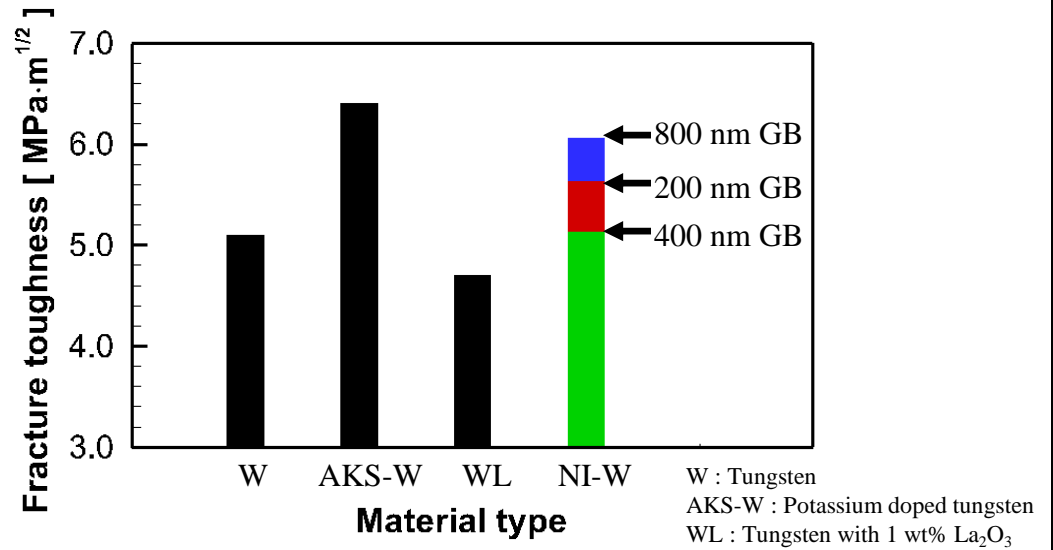
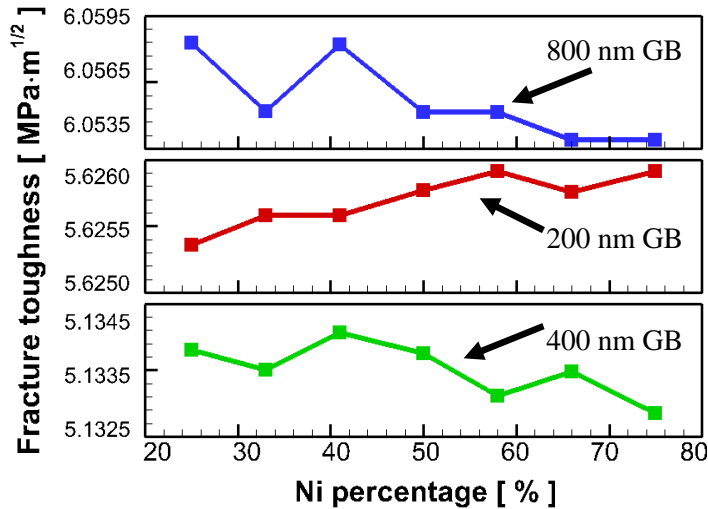
➤ Fracture toughness analysis



Fracture toughness in crack initiation

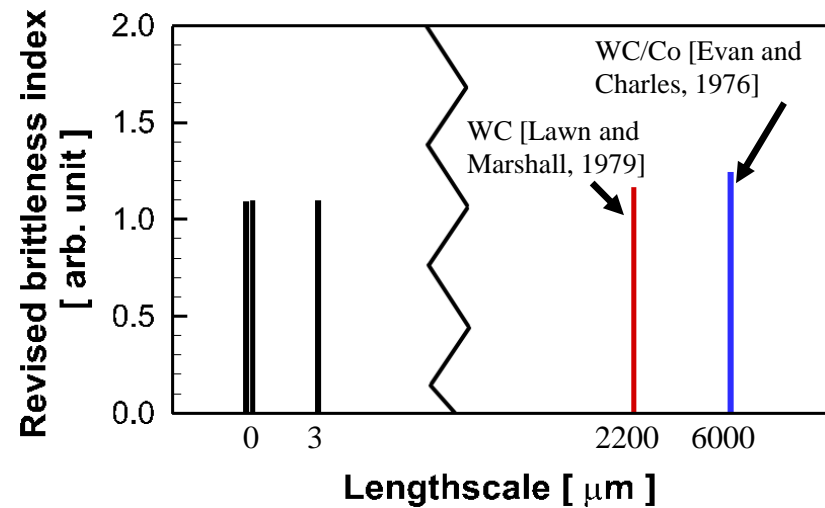
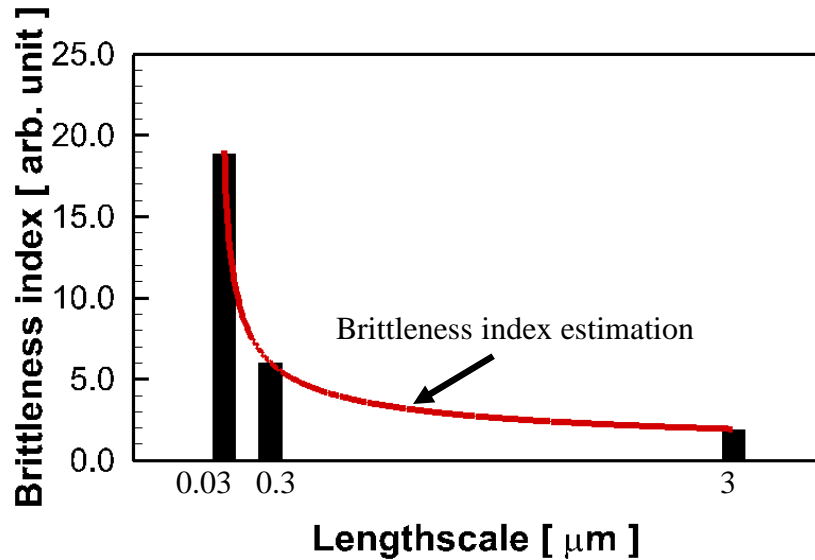


Fracture toughness inside the GB

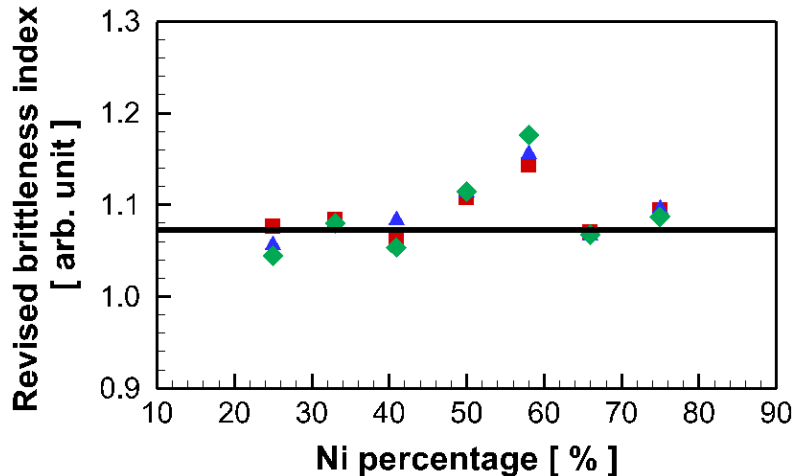


[B. Gludovatz and et al., 2010]

➤ Brittleness index of GBs



Effect of length-scale : $B = 3.3L^{-1/2}$



$$B^* = \frac{H}{K_c} \cdot \frac{1}{\alpha} \sqrt{L}$$

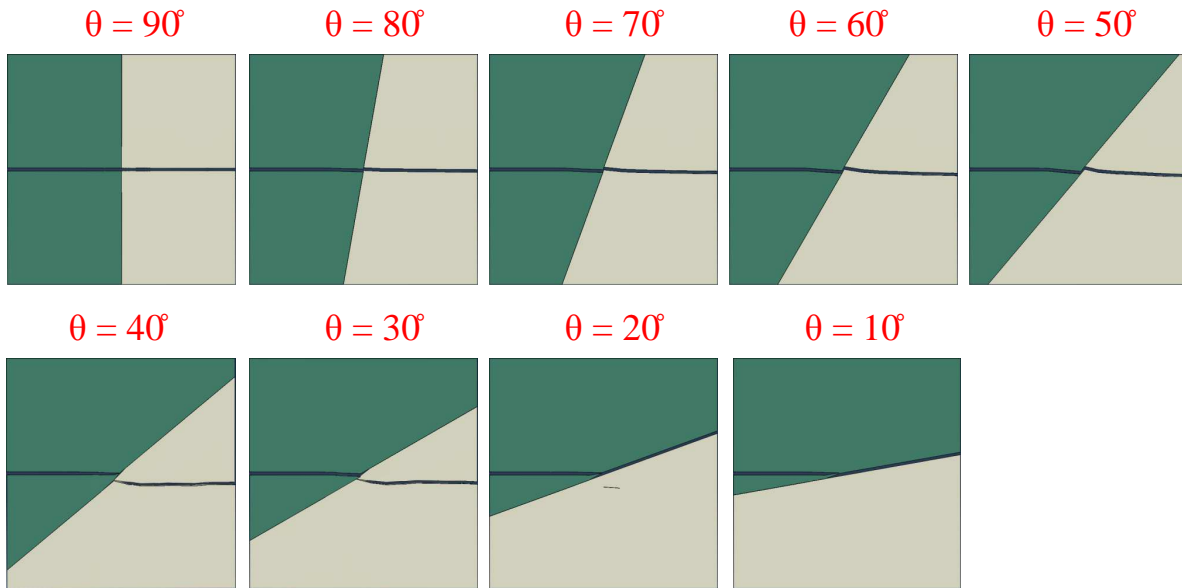
$\alpha = 3.3$ for W-Ni

Nomenclature

B^*	brittleness index (no unit)
L	lengthscale (μm)
T	max. tensile strength (fracture strength)
H	hardness (GPa)
K_c	fracture toughness ($\text{MPa m}^{1/2}$)
t	GB thickness (μm)
p	Ni fraction (no unit)

- Measurement of GB embrittlement has been obtained using the revised brittleness index.
- This provides an absolute range of qualitative measurement to describe the brittleness without considering the length scale limitations.

➤ Crack propagation in different angled GBs



- Inter-granular failure is represented as 1
- Trans-granular failure is represented as -1

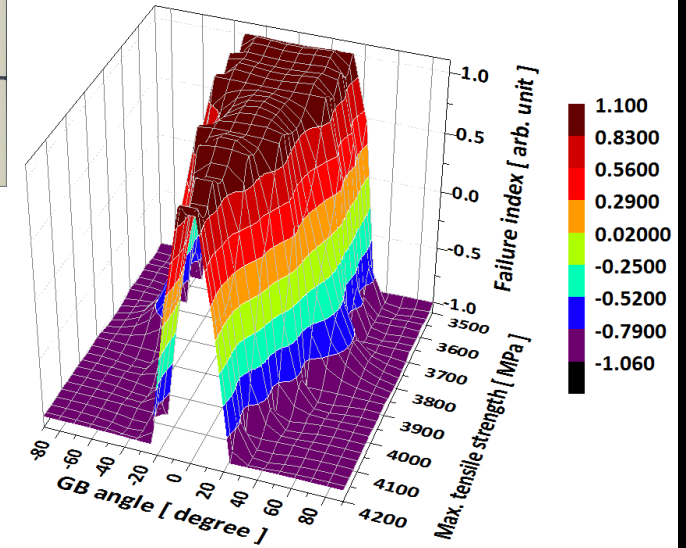
❖ **Failure index** : An index (between -1 and 1) to describe failure type, which can be either inter-granular failure or trans-granular failure.

$$FI = a + b \frac{T_{GB}}{T_{Grain}} + c \theta^2$$

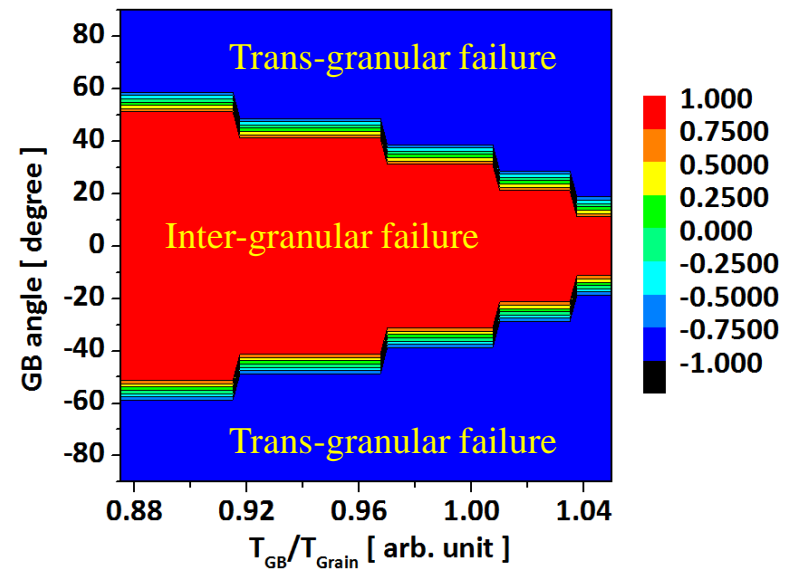
$a = 4.45$
 $b = -4.2$
 $c = -0.00024$

Using the Heaviside function

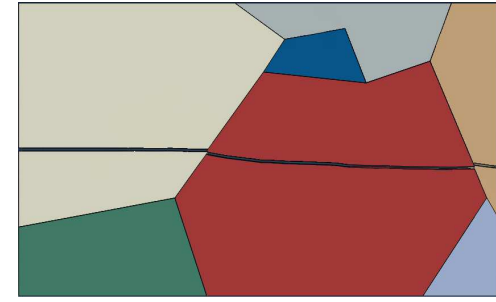
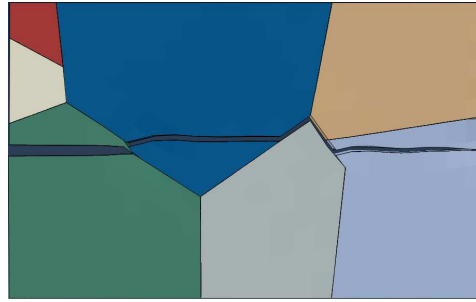
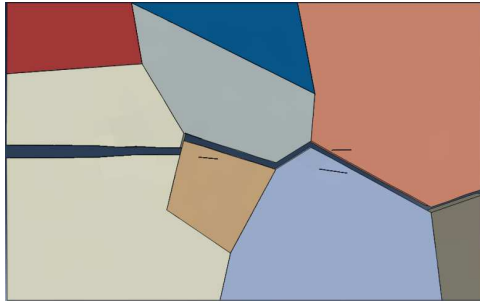
$$H[FI] = \begin{cases} 1, & FI \geq 0 \\ -1, & FI < 0 \end{cases}$$



GB angle from -90 to 90 degree



➤ Validation and Conclusion

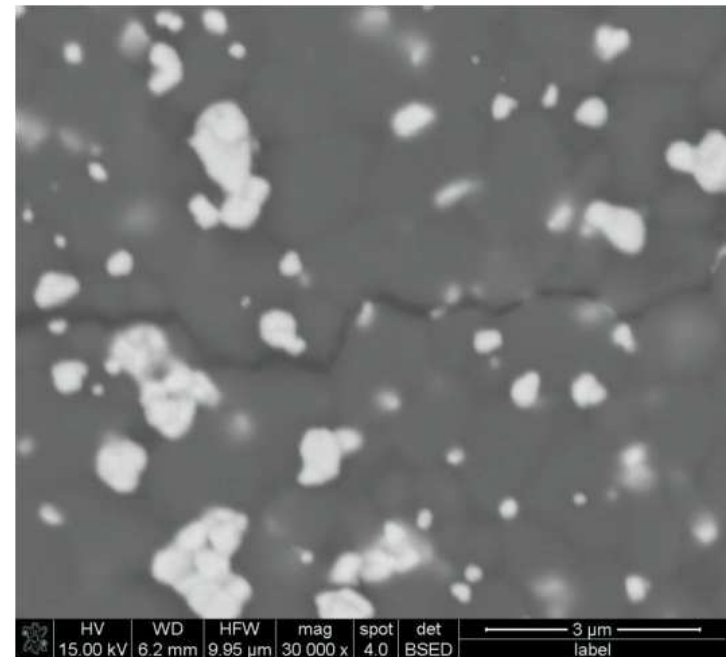


- Perfect inter-granular failure has occurred.
- Contains crack path with maximum GB angle of 67° .
- GB strength property can be predicted.

$$FI = a + b \frac{T_{GB}}{T_{Grain}} + c \theta^2$$

- According to the failure index prediction, given microstructure has max. tensile strength ratio between GB and grain as $T_{GB} \leq (0.803) \cdot T_{Grain}$.

✓ For various failed morphologies of polycrystalline W-Ni, GB's strength property can be predicted using the derived failure type criteria.

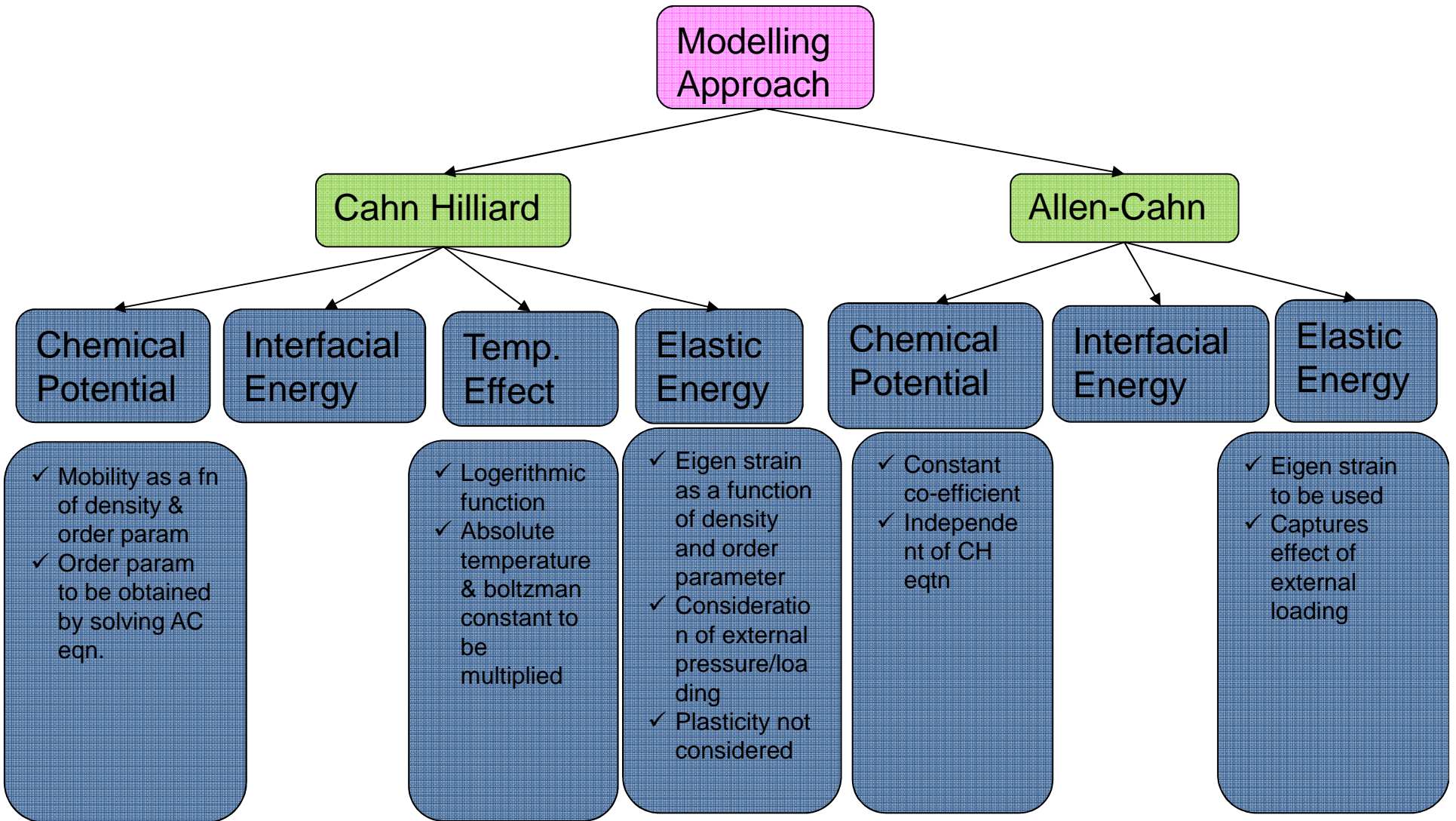


[Zbigniew Pedzich, 2012]

Evolution: Previous Works

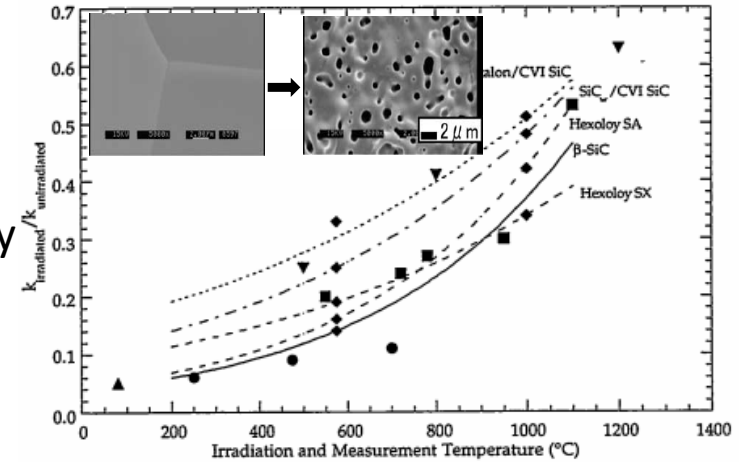
- Microstructure evolution has been observed through experimental studies
Groza, 2000; Hong, 2003; Dahl, 2007
- Simulation developed replicating the whole sintering process
Maizza, 2007; Vanmeensel, 2005
- Kinetic Monte Carlo simulation applied to microstructural evolution: Probabilistic approach, depends on random sampling
Olevsky, 2004
- Phase field modeling has been done to identify sintering mechanisms, external loading not considered
Wang, 2006; Liu, 2011; Deng, 2012
- Consolidation kinetics has been captured experimentally
Bruson, 1984; Grigoryev, 2009; Tang, 2013

Modeling Approach



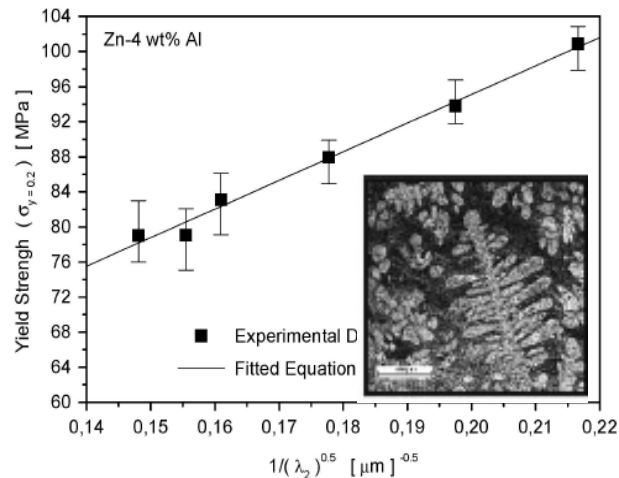
Impact of Microstructure Evolution

- Grain growth due to irradiation, annealing reduces maximum tensile strength of a material
- Formation of void impacts the thermal conductivity of a material
- Solidification reduces the yield strength

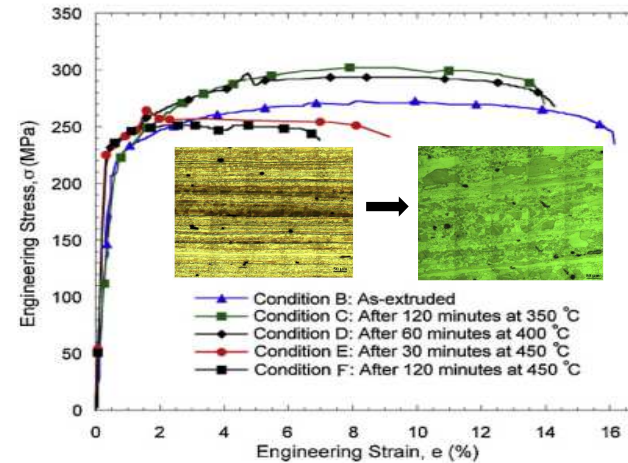


Impact of Irradiation

[Youngblood, 1996; Takamura, 2004]



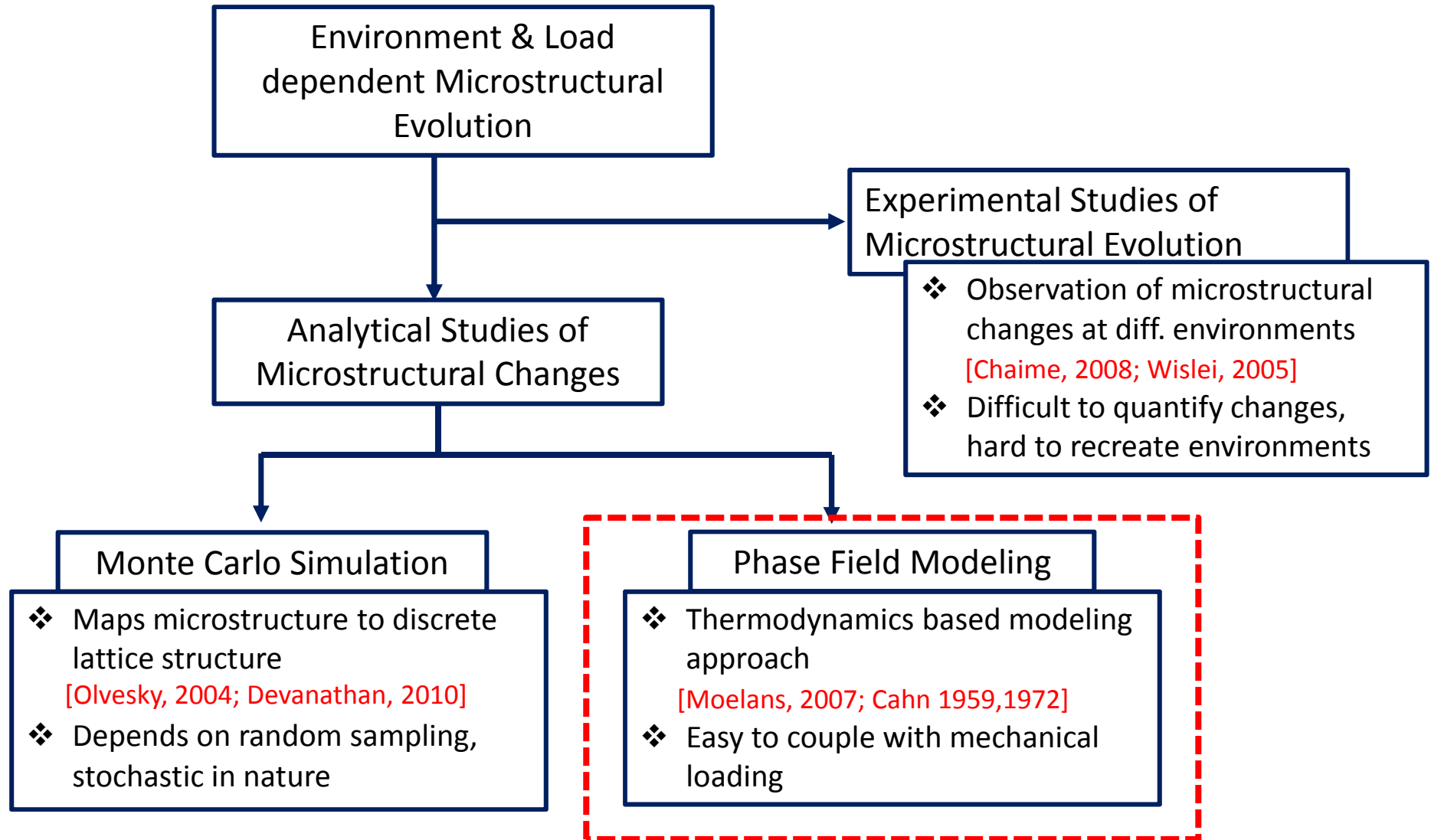
Change in yield strength due to solidification [Wislei, 2005]



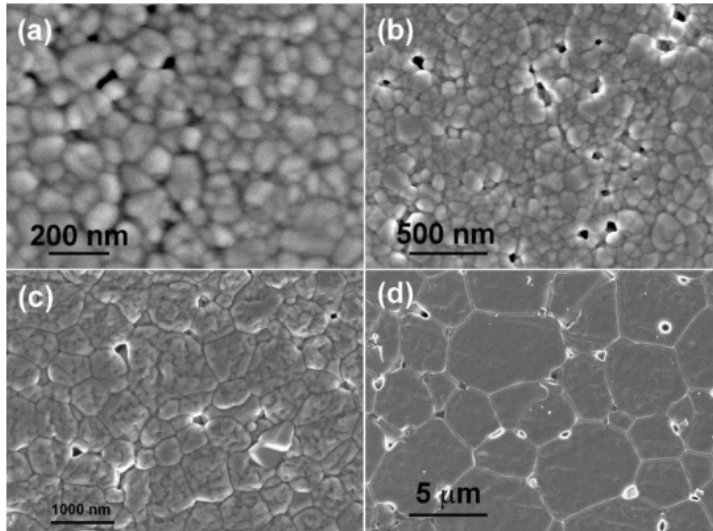
Impact Of Grain growth

[Ramamurty, 2009]

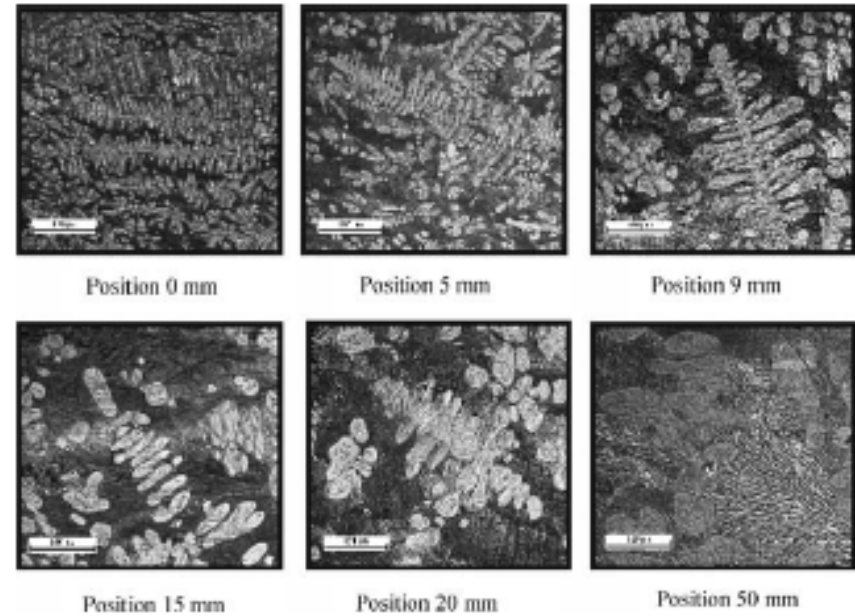
Study of Microstructural Evolutions



Experimental Observations



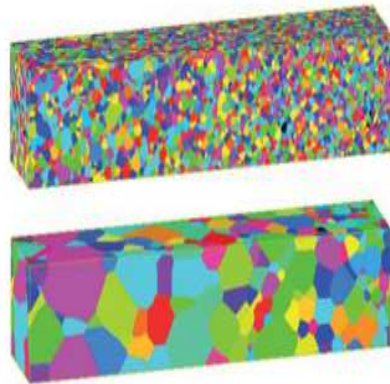
Grain growth of Y_2O_3 at Different Temp.
[Chaime, 2008]



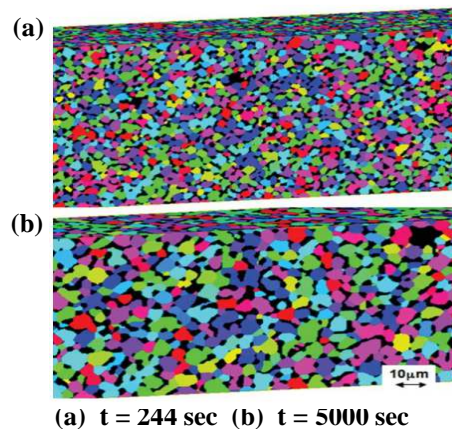
Solidification Process in ZA₄
[Wislei, 2005]

Kinetic Monte Carlo Simulation

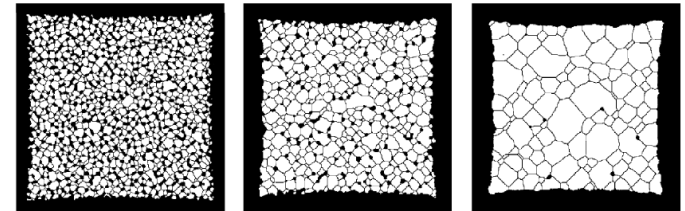
- A statistical-mechanical model that populates a lattice with an ensemble of discrete particles to represent and evolve microstructure.
- KMC can simulate kinetics and topology of grain growth: anisotropic grain growth, recrystallization, particle sintering, etc.



Grain growth due to temperature gradient
[Devanathan, 2010]



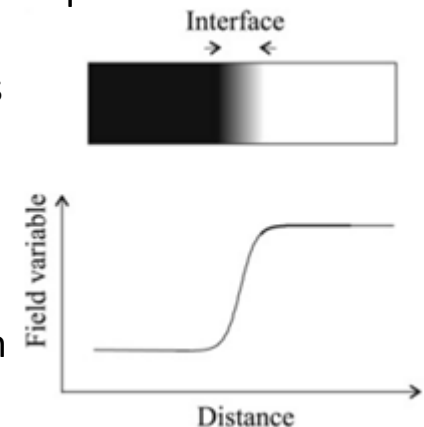
Grain (color) and pore (black) growth
[Devanathan, 2010]



KMC simulation of powder compaction
[Olvesky, 2004]

Phase Field Modeling

- In Phase Field, microstructure is assumed to be a thermodynamically unstable structure which evolves in time and space for reaching equilibrium by minimizing the free energy
- Microstructural features such as concentration of phases, grain orientation etc. are identified as phase field variables.
- Within the grains, the phase field variables have nearly constant values. The interface between two grains is defined as a narrow region where the phase-field variables gradually vary between their values in the neighboring grains - A diffuse-interface description
- No need to track the interface positions explicitly by means of mathematical equations
- The evolution of the phases, shape of the grains, positions of the interfaces are implicitly given by the evolution of the phase-field variables.
- Versatile technique for simulating microstructure evolution in various material processes at the mesoscale: solidification, precipitate growth, solid-state phase transformation, martensitic transformation, grain growth

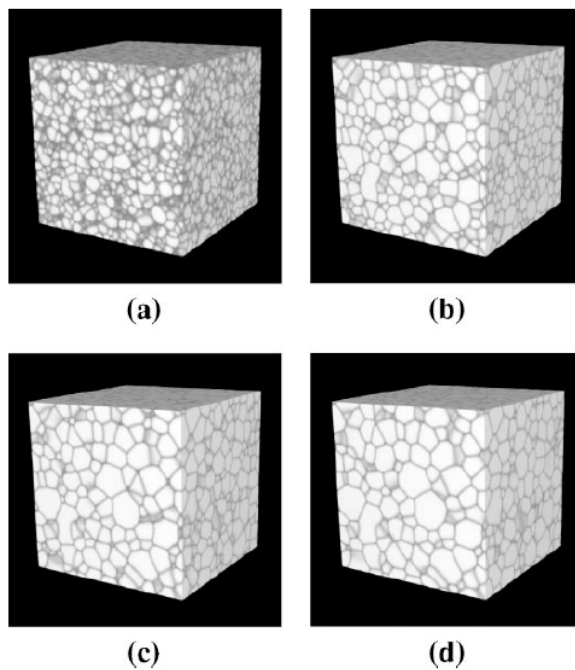


Diffuse Interface

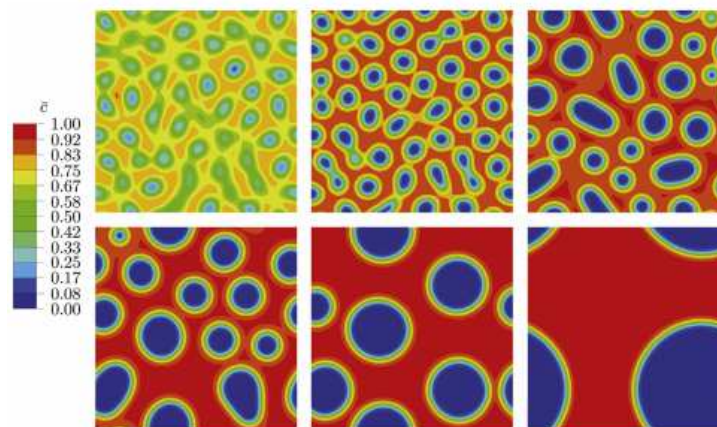
[Moelans, 2007]

Phase Field Modeling

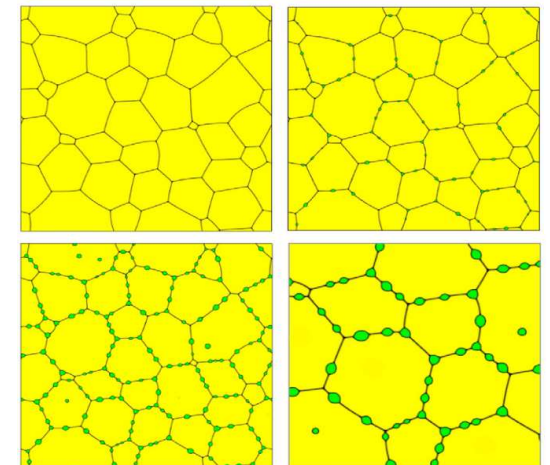
- A deterministic, continuum, thermodynamic model that describes the microstructure and its evolution in terms of continuum phase-field variables



Grain growth model
[Chen, 2002]



Phase separation through
spinodal decomposition
[Anand, 2013]

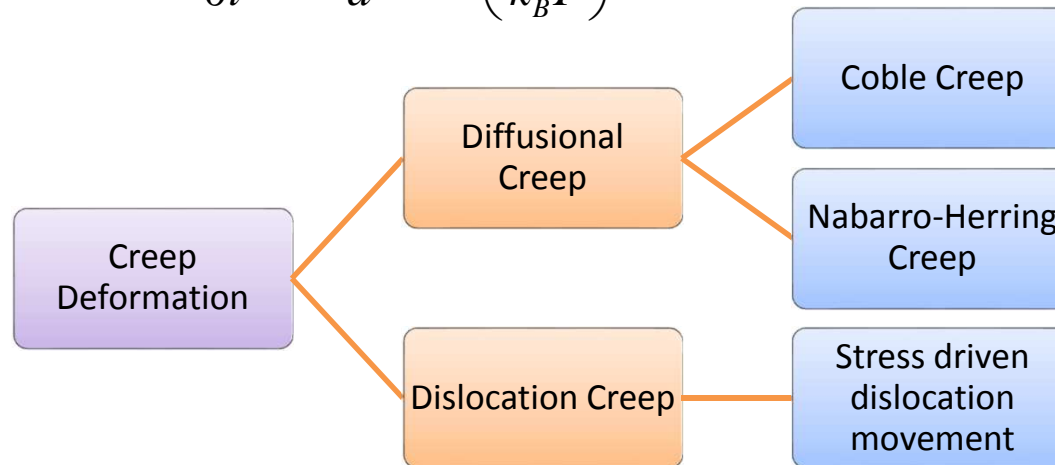


Nucleation and growth of
intergranular gas bubbles
[Millett, 2011]

Creep Deformation

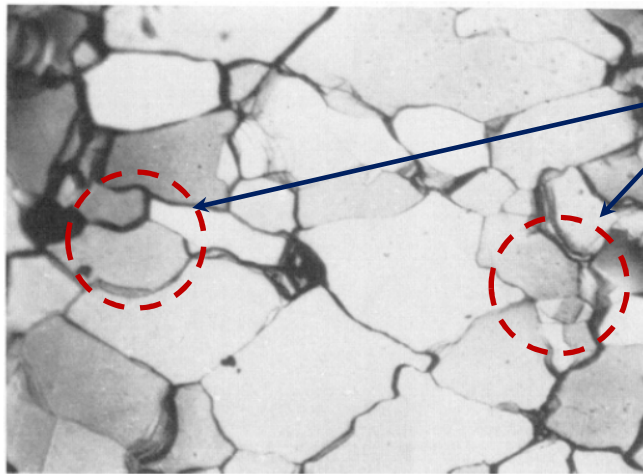
- Creep is permanent deformation of materials due to long term exposure to high temperature and loading.
- Creep may occur due to dislocation pile up or plastic flow or vacancy diffusion along lattice sites & grain boundaries in a material. [Ashby, 1982]
- Creep is expressed with power law as,

$$\frac{\partial \epsilon}{\partial t} = C \frac{\sigma^n}{d^b} \exp\left(\frac{-Q}{k_B T}\right)$$



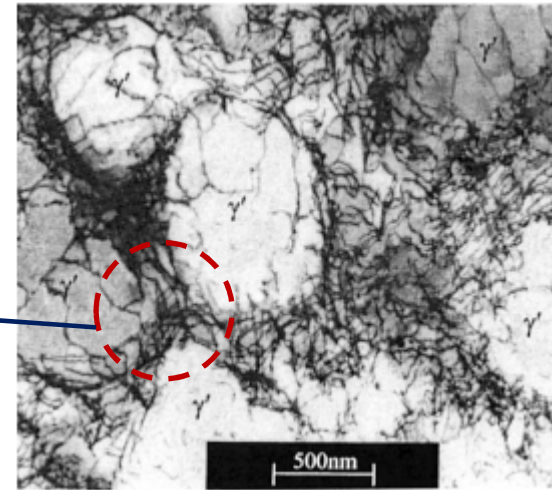
Creep Mechanisms

Microstructural Changes



Curved GB due to
GB sliding & creep

Dislocation climb
near interface



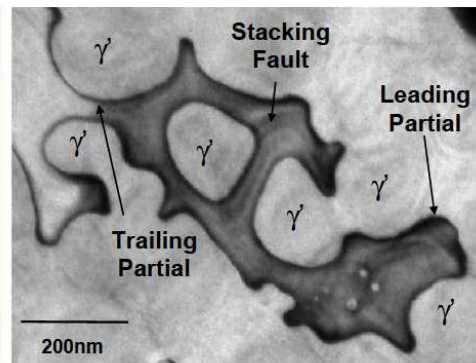
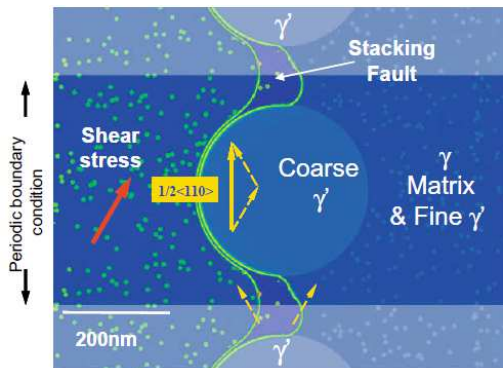
GB Sliding Creep
[Gifkins, 1974]

Dislocation Creep
[Sajjadi, 2002]

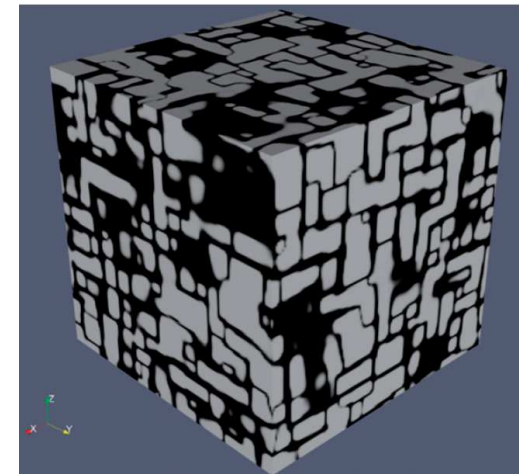
- Creep mechanism depends on grain size, temperature & applied loads
- Diffusion creep is temperature driven whereas dislocation creep is stress driven
[Weertman, 1955; Pierro, 1977]
- Creep leads to grain growth and GB sliding
- Microstructural evolution due to long-term creep not been studied analytically

Phase Field & Creep

- Ni alloys are used at high temperature and are subjected to creep
- Coarsening of γ' phase in Ni-Al Alloy has been studied through phase field approach [Wang, 2009]
- Kim-Kim-Suzuki method has been adopted to simulate creep at small scale [Zhou, 2010]
- Grain orientation, slip plane, plastic flow has been considered into modeling
- Effect of creep has not been shown explicitly



Coarsening due to Creep
[Wang, 2009]



γ' Rafting & Creep
[Zhou, 2010]

Modeling Formulation

[Moelans, 2007]

➤ Free energy can be represented as,

$$F = \int \left[f_{bulk}(c, \eta) + f_{el}(c, \eta) + \frac{\kappa_c}{2} |\nabla c|^2 + \frac{\kappa_\eta}{2} |\nabla \eta|^2 \right] dV$$

$f_{bulk}(c, \eta)$: free chemical energy of the material,

κ_c and κ_η : gradient coefficients,

c : phase field variable/phase concentration

η : order parameter (crystallographic orientation of phases)

f_{el} : strain energy

➤ Phase Field Evolution,

Cahn-Hilliard Equation:
$$\frac{\partial c}{\partial t} = \nabla \cdot M \nabla \frac{\delta F}{\delta c} = \nabla \cdot M \nabla \left(\frac{\delta f_{bulk}}{\delta c} + \frac{\delta f_{el}}{\delta c} - k_c \nabla^2 c \right)$$

Allen-Cahn Equation:
$$\frac{\partial \eta_i}{\partial t} = -L \frac{\delta F}{\delta \eta_i} = -L \left(\frac{\delta f_{bulk}}{\delta \eta_i} + \frac{\delta f_{el}}{\delta \eta_i} - k_{\eta_i} \nabla^2 \eta_i \right)$$

Visco-plastic Modeling

- Plastic energy is calculated based on two internal variables related to kinematic and isotropic hardening.

- The viscoplastic energy contribution is formulated as follows, [Cottura, 2012]

$$F_{vp}(\alpha, p) = \int_V \frac{1}{3} C \alpha : \alpha + \frac{1}{2} H p^2 + \frac{1}{2} A |\nabla p|^2 dV$$

where, α and p are the hardening parameters. C , H & A are constants.

- Linear isotropic hardening is related to plastic strain as,

$$\dot{p} = \sqrt{\frac{2}{3} \dot{\epsilon}_p : \dot{\epsilon}_p}$$

- Plastic strain along with creep rate can be estimated from evolution of viscoplastic energy.
- Total free energy in the phase field is modified to accommodate viscoplastic energy,

$$F = F_{ch}(c, \eta_i) + F_{el}(c, \eta_i, \epsilon_{el}) + F_{vp}(\alpha, p)$$

- Mobility values are converted using time scales such that microstructural evolution is obtained in hours/years

Visco-plastic Modeling

- Yield surface,

$$f = \frac{K}{N+1} \left\langle \frac{J_2(\underline{\sigma} - \underline{X}) - R_0 - R}{K} \right\rangle^{N+1}$$

$$\underline{X} = \frac{2}{3} C \underline{\alpha} \text{ and } R = Hp - A\Delta p$$

- Dissipation Potential,

$$\Omega = \int_V \tilde{\Omega} \left[J_2(\underline{\sigma} - \underline{X}) - R_0 - R + \left(\frac{D}{2C} J_2^2(\underline{X}) - \frac{2DC}{9} J_2^2(\underline{\alpha}) \right) \right] dV$$

where, α and p are the hardening parameters. C , D , H are material parameters. X is the back stress.

- Hardening flow rules for internal variables,

$$\dot{p} = \left\langle \frac{J_2(\underline{\sigma} - \underline{X}) - R_0 - R}{K} \right\rangle^N$$

$$\dot{\underline{\varepsilon}}^p = \frac{3}{2} \dot{p} \frac{\underline{\sigma} - \underline{X}}{J_2(\underline{\sigma} - \underline{X})}$$

$$\dot{\underline{\alpha}} = \dot{\underline{\varepsilon}}^p - D \underline{\alpha} \dot{p}$$

$$J_2(\underline{\sigma}) = \sqrt{\frac{3}{2} \underline{\sigma}' : \underline{\sigma}' \text{ with } \underline{\sigma}' = \underline{\sigma} - \frac{1}{3} \text{Tr}(\underline{\sigma}) \underline{I}}$$

Elastic Energy Formulation

[Moelans, 2007]

➤ Elasticity constants are assumed to vary with phase concentration

➤ Elastic strain is calculated as: $\boldsymbol{\varepsilon}_{ij}^{el} = \boldsymbol{\varepsilon}_{ij}^{total} - \boldsymbol{\varepsilon}_{ij}^0$ with $\boldsymbol{\varepsilon}_{ij}^0$: eigenstrain

➤ Total strain is estimated from displacements, $\boldsymbol{\varepsilon}_{kl}^{total}(\mathbf{r}) = \frac{1}{2} \left[\frac{\partial u_k(\mathbf{r})}{\partial r_l} + \frac{\partial u_l(\mathbf{r})}{\partial r_k} \right]$

➤ Local elastic stress, $\vec{\sigma}_{ij}(\mathbf{r}) = C_{ijkl}(\vec{\mathbf{r}}) \boldsymbol{\varepsilon}_{kl}^{el}(\vec{\mathbf{r}})$

➤ Considering the fact that mechanical equilibrium is obtained much before the chemical equilibrium, strain is obtained by solving the equilibrium equation,

$$\frac{\partial \sigma_{ij}}{\partial r_j} = 0$$

➤ Elastic Energy (f_{el})

$$f_{el} = \frac{1}{2} \int_V C_{ijkl}(\mathbf{r}) \boldsymbol{\varepsilon}_{ij}^{el} \boldsymbol{\varepsilon}_{kl}^{el} d\mathbf{r}$$

Here, $u_k(\mathbf{r})$: displacement component

$\boldsymbol{\varepsilon}_{kl}^{el}(\mathbf{r})$: elastic strain

$C_{ijkl}(\vec{\mathbf{r}})$ elastic constants

$\vec{\sigma}_{ij}(\mathbf{r})$: effective stress

Numerical Simulation

Phase Field Variable Update, Cahn-Hilliard

[Zhang, 2013; Tonks, 2012]

Split Version:
$$\frac{\partial c}{\partial t} = \nabla \cdot (M \nabla \mu) \quad \mu = \frac{\delta f_{bulk}}{\delta c} + \frac{\delta f_{el}}{\delta c} - k_c \nabla^2 c$$

Weak Form:
$$\left(\frac{\partial c}{\partial t}, \psi_m \right) = (M \nabla \mu, \nabla \psi_m) - \langle M \nabla \mu \cdot \vec{n}, \psi_m \rangle$$

$$(\mu, \psi_m) = \left(\frac{\delta f_{bulk}}{\delta c} + \frac{\delta f_{el}}{\delta c}, \psi_m \right) + (k_c \nabla c, \nabla \psi_m) - \langle k_c \nabla c \cdot \vec{n}, \psi_m \rangle$$

with mobility
$$M = \frac{DV_m}{k_B T}$$

where, diffusivity,
$$D = D_0 \exp\left(\frac{-Q}{k_B T}\right)$$

Order Parameter Update, Allen-Cahn

Strong Form:
$$\frac{\partial \eta_i}{\partial t} = -L \left(\frac{\delta f_{bulk}}{\delta \eta_i} + \frac{\delta f_{el}}{\delta \eta_i} - k_{\eta_i} \nabla^2 \eta_i \right)$$

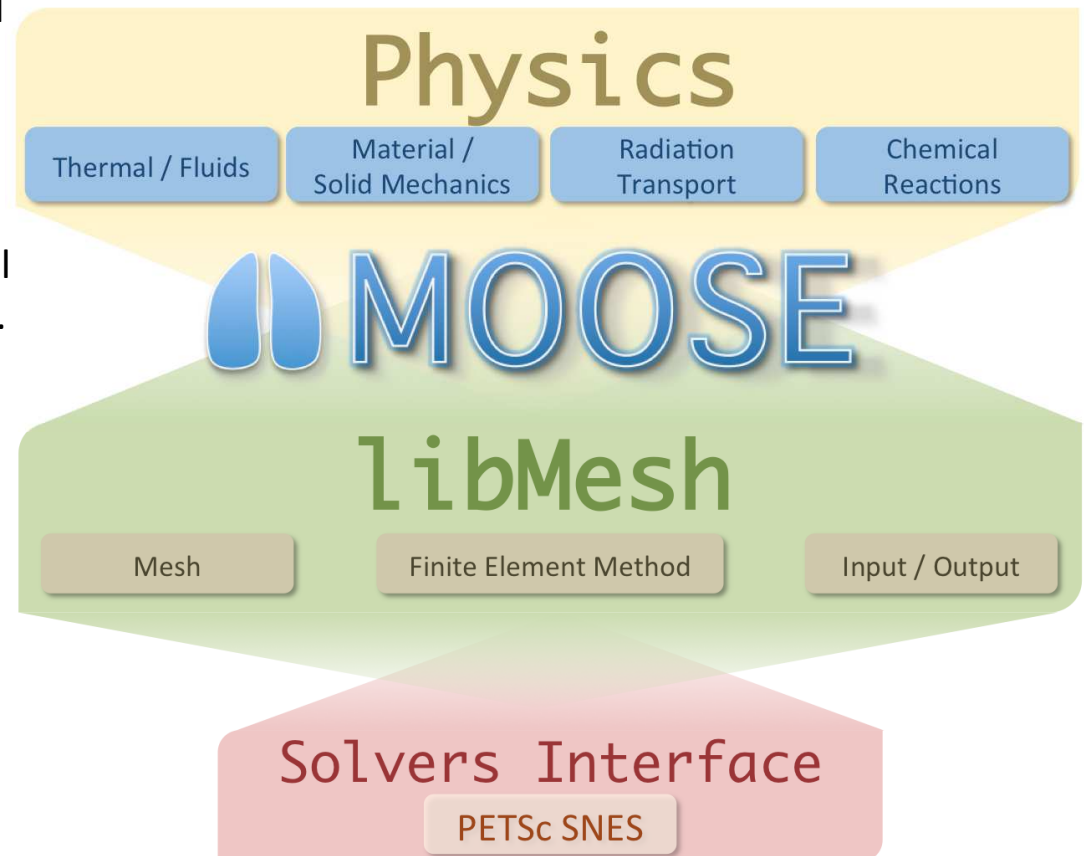
Weak Form:
$$\left(\frac{\partial \eta_i}{\partial t}, \psi_m \right) = -L \left(\frac{\delta f_{bulk}}{\delta \eta_i} + \frac{\delta f_{el}}{\delta \eta_i}, \psi_m \right) + L (k_{\eta_i} \nabla \eta_i, \nabla \psi_m) - L \langle k_{\eta_i} \nabla \eta_i \cdot \vec{n}, \psi_m \rangle$$

where, L is Allen-Cahn mobility

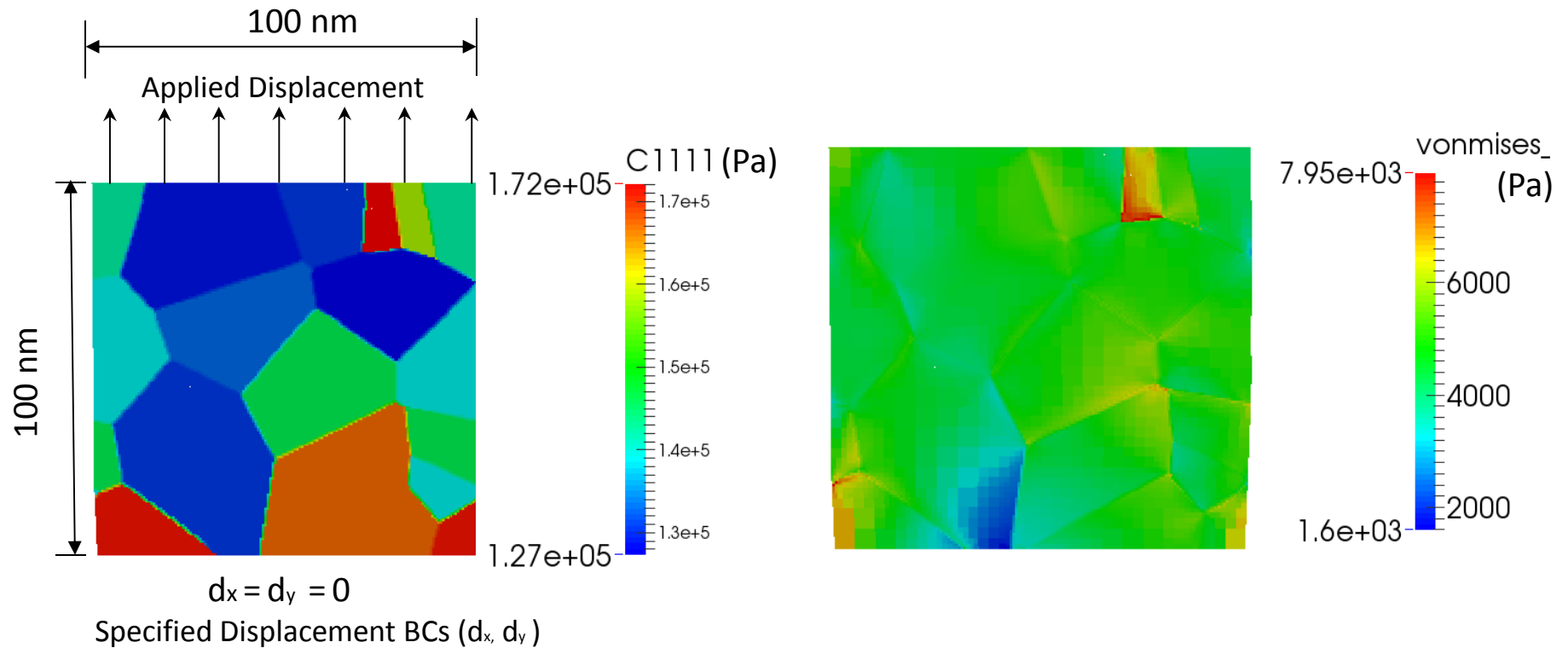
Simulation Tool

[mooseframework.org]

- MOOSE (Multiphysics Object Oriented Simulation Environment) frameworks used for current simulation, an open source codes developed by Idaho National Lab (INL).
- Finite element based solver to solve partial differential equation of any kind and order.
- Nonlinear solvers from Petsc, automatic time & mesh adaptivity.
- Inbuilt modules provides capability of phase field, solid mechanics, heat conduction etc. compatible with each other
- C++ based coding capable of handling complicated mathematical formulations/operations.



Microstructure Dependence

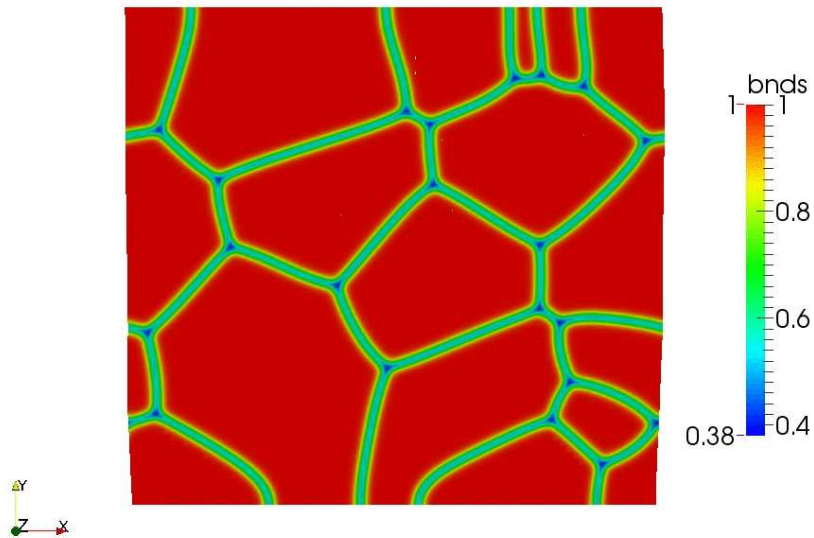


Elastic Properties & BCs

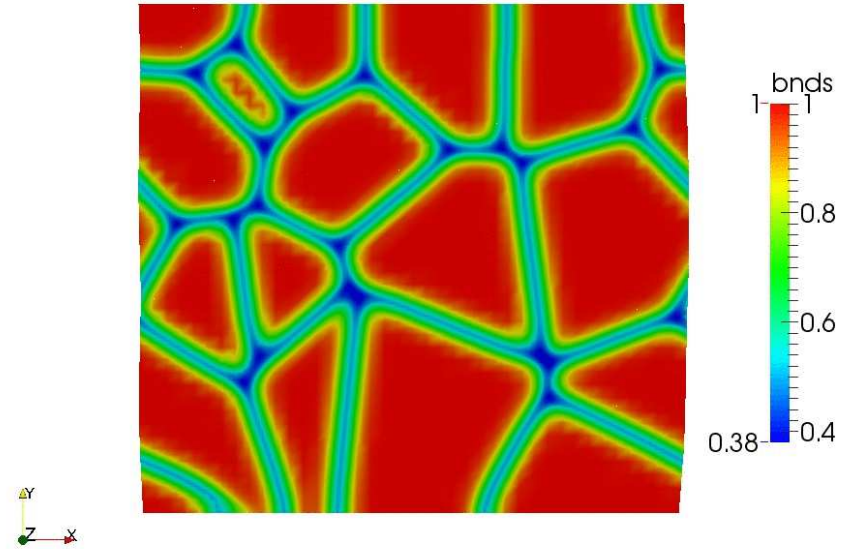
Vonmises Stress Response

- Mechanical properties depend on grain orientation, so as the stress-strain profile
- Grain growth impacts the change in stress experienced by the grains

Microstructural Changes

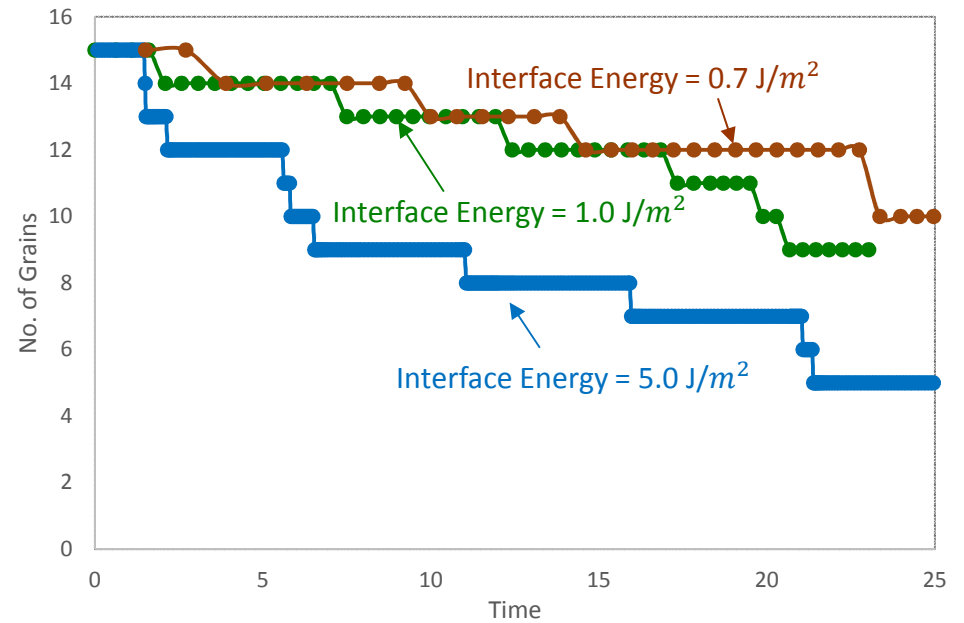
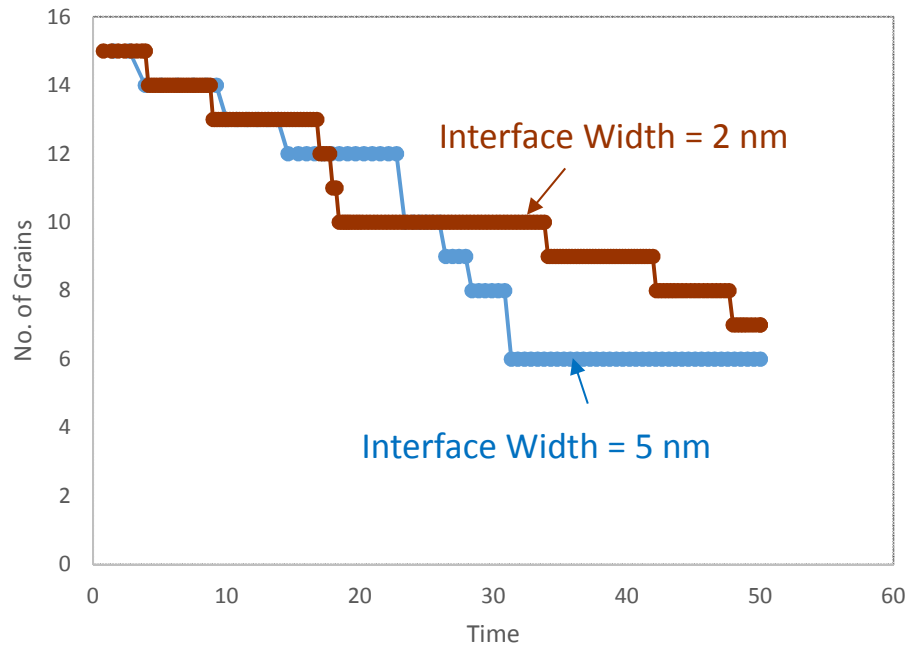


**Grain growth over time
(simulation time = 50 sec;
Interface width = 2 nm)**



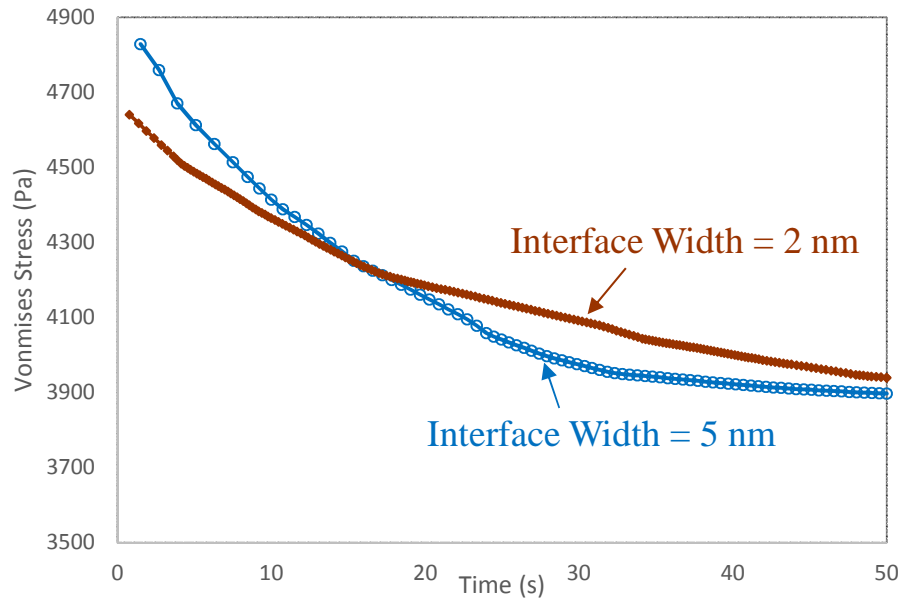
**Grain growth over time
(simulation time = 50 sec;
Interface width = 5 nm)**

Grain Growth

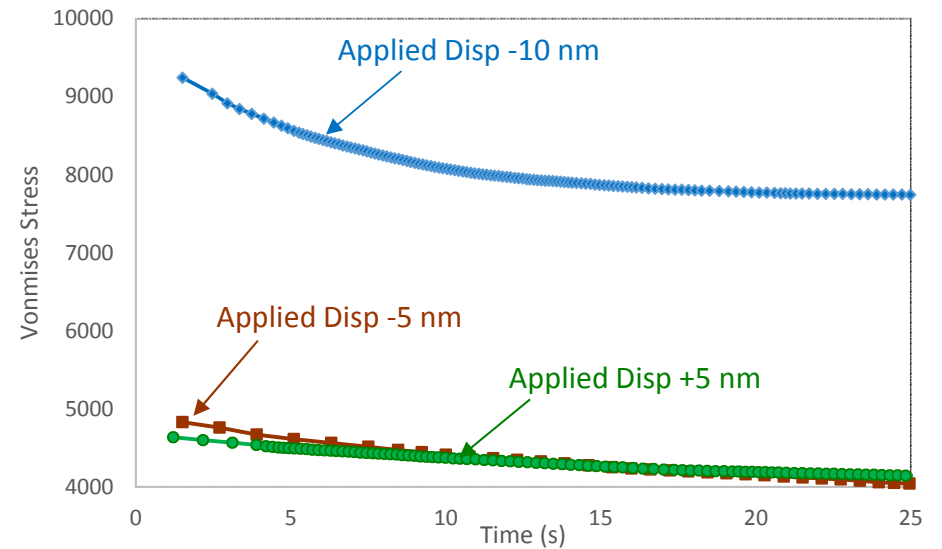
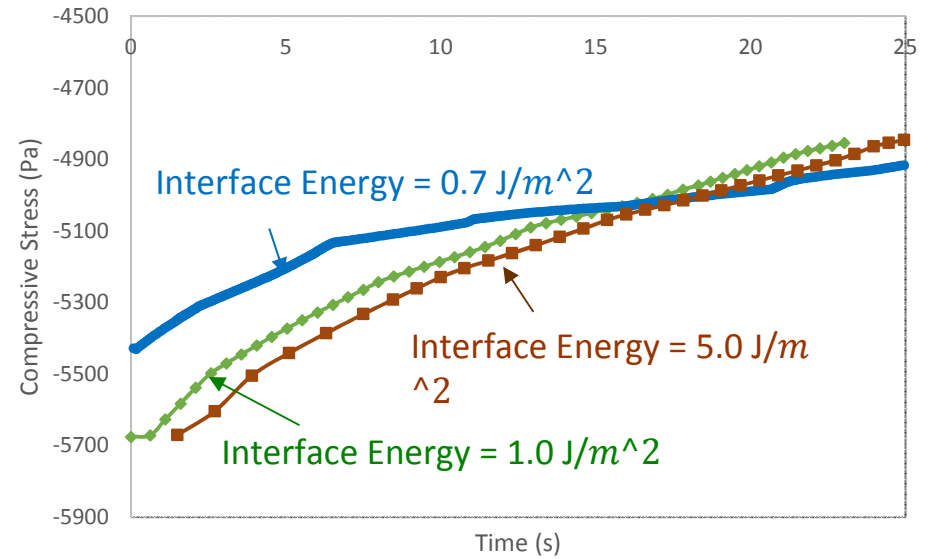


- Rate of grain growth increases with increase in interfacial width and its energy
- Final no. of grains decreases and average grain size increases over time

Stress Variation



- Rate of change in stress at initial stage changes with interfacial width and its energy
- Over a period of time grain growth reaches a saturation level and stress stabilizes



Next Steps

Evaluate Creep deformation mechanisms due to long-term loading



Develop creep model based on compressive load

Nano-indentation experiments on sintered materials



Obtain mechanical properties & creep deformation mechanisms

Compare & validate modeling approach with Experimental outcomes



Extend model to tensile loading for generic creep deformation prediction

Validation Plan

- Obtain time vs. depth curve from simulation and compare with experimental curves
- Obtain deformation mechanism and compare with experimental mechanisms predicted from stress exponent
- Obtain Stress-strain curve, mechanical properties, compare with experimental data

Experimental Design

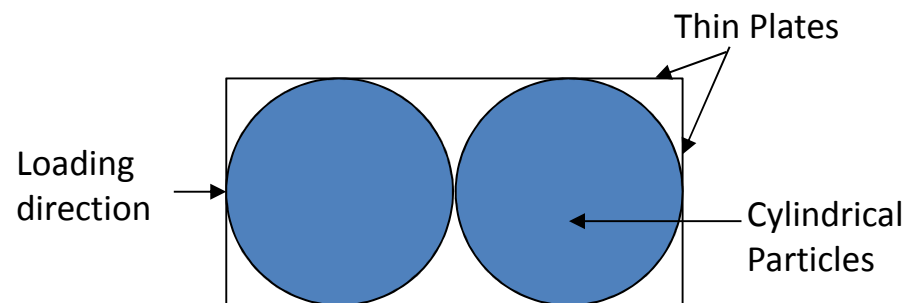
❑ Process requirements:

- Load/Pressure: 400 Mpa
- Temperature: 1400 C
- Time: 5 hours in case of normal process
- Sintering Criteria: Ratio of self diffusion to the particle radius (D/r) should be greater than $4e-8$ m/s

[Heuer, 1982]

❑ Issues Identified:

- Difficult to re-create sintering conditions
- Only deformation can be observed, no diffusion
- Obtained stress/temp will not be related to sintering process
- Deformation (bending) of the surrounding plate is possible due to applied load



Cross-section of the experimental set-up proposal

Summary

- All Tasks on Schedule
- A Grain Boundary Diagram Based Approach for long term GB evolution identified and linked with such predictions
- A Brittleness Index parameter identified to predict effect of GB on microstructural Strength
- Control sample manufacturing process established
- In-situ and ex-situ experimentation protocols established and experiments performed
- 5 international journal publications, 1 PhD graduate, 3 supported students with grant in second year